İSTANBUL TECHNICAL UNIVERSITY ★ INSTITUTE OF SCIENCE AND TECHNOLOGY

ESTIMATION OF MATERIAL COEFFICIENTS OF SOFT TISSUES USING EXPERIMENTAL DATA AND INVERSE FINITE ELEMENT METHOD

M.Sc. Thesis by
Gülnur DEMİR

Department : Computational Science and Engineering

Programme : Computational Science and Engineering

Thesis Supervisor: Prof. Dr. M. Serdar ÇELEBİ

DECEMBER 2010

İSTANBUL TECHNICAL UNIVERSITY ★ INSTITUTE OF SCIENCE AND TECHNOLOGY

ESTIMATION OF MATERIAL COEFFICIENTS OF SOFT TISSUES USING EXPERIMENTAL DATA AND INVERSE FINITE ELEMENTS METHOD

M.Sc. Thesis by
Gülnur DEMİR
(702071008)

Date of submission : **20 December 2010**
Date of defence examination: **26 January 2011**

Supervisor (Chairman) : **Prof. Dr. M. Serdar ÇELEBİ (ITU)**
Members of the Examining Committee : **Assist. Prof. Dr. F. Aylin KONUKLAR (ITU)**
Prof. Dr. Zahit MECİTOĞLU (ITU)

DECEMBER 2010

İSTANBUL TEKNİK ÜNİVERSİTESİ ★ FEN BİLİMLERİ ENSTİTÜSÜ

YUMUŞAK DOKULARIN MALZEME KATSAYILARININ DENEYSEL VERİLER VE TERSİNE SONLU ELEMANLAR YÖNTEMİ KULLANILARAK HESAPLANMASI

YÜKSEK LİSANS TEZİ
Gülnur DEMİR
(702071008)

Tezin Enstitüye Verildiği Tarih : **20 Aralık 2010**
Tezin Savunulduğu Tarih : **26 Ocak 2011**

Tez Danışmanı : **Prof. Dr. M. Serdar ÇELEBİ (İTÜ)**
Diğer Jüri Üyeleri : **Yrd. Doç. Dr. F. Aylin KONUKLAR (İTÜ)**
Prof. Dr. Zahit MECİTOĞLU (İTÜ)

ARALIK 2010

FOREWORD

I would like to thank Prof. Dr. M. Serdar Çelebi for being my advisor and mentor during this research.

Next, I would like to express my deep appreciation to Assis. Prof. Dr. Fırat Doğan who have kindly shared his knowledge and wisdom with me.

I would also like to thank all my friends and collegues in Computational Science and Engineering department, but especially to Şenol Pişkin, Hasret Türkeri, and Esra Baltaoğlu.

I would like to extend my thanks to the staff of the Tissue Laboratory in Biomedical Engineering department of Boğaziçi University, Assis. Prof. Dr. Can Yücesoy, Assis. Prof. Dr. Özgür Tabakoğlu, and Nermin Topaloğlu for opening their resources to my use, for their help and kindness.

Finally, I would like to express my greatest gratitude to my family for their love and support over so many years. Special thanks to my brother Dr. Hasan Demir for believing me in this research, and for sharing his knowledge with me.

I owe thanks to anybody who had a word or who wasted a moment for this work.

This work is supported by ITU Scientific Research Project Unit (ITU BAP).

December 2010

Gülnur Demir

Mathematics Engineer

TABLE OF CONTENTS

Page

ABBREVIATIONS

App **:** Appendix
FE **:** Finite Element
FEA **:** Finite Element Analysis
FEM **:** Finite Element Method
GN **:** Gauss-Newton
ITU **:** Istanbul Technical University
LM **:** Levenberg-Marquardt

LIST OF TABLES

Page

LIST OF FIGURES

Page

ESTIMATION OF MATERIAL COEFFICIENTS OF SOFT TISSUES USING EXPERIMENTAL DATA AND INVERSE FINITE ELEMENT METHOD

SUMMARY

In this thesis a set of indentation experiments conducted on bovine liver and on a synthetic material are presented and the material coefficients of the materials are computed using the test data via inverse finite elments algorithm.

The literature in this area has been in need of determined material coefficients of soft biological tissues. There are already published values for various soft tissues, however, testing environments and conditions affect the results because soft biological tissues display different behaviour with respect to the vitality, the storage conditions, or the boundary conditions. Also, determining the accurate material model of the tissue is important; since the coefficients of the material model that is assigned to the tissue are computed in this process. On the other hand, the synthetic material was involved in the study with a prediction that it would present similar mechanical properties with soft biological tissues. Artificial materials eases the validation of the simulation models by providing any data for any condition if they are mechanically similar to the subject tissue.

In this study, static indentation experiments and relaxation experiments are performed on the synthetic gel which is Aquaflex Ultrasound Gel Pad and on bovine liver. The experiements on bovine liver are performed ex-vivo. The data obtained from the experiments are used to determine the coefficients for various material models by either curve fitting or by inverse finite element algorithm. For the Aquaflex Ultrasound Gel, the static indentation test data is fitted to the Mooney-Rivlin and Yeoh type material models and the related coefficients are computed. The ramp-hold test data is fitted to the Prony series expansion of the relaxation function for the viscoelastic model and the coefficients are computed. Both data is also used for coefficient determination via inverse finite element method. For this purpose, the simulation models of the materials and the experiments for each case are constructed by a finite element modeling software. These processes are also repeated with the

data obtained from the bovine liver tests. In order to anaylze the axial differences in terms of mechanical behaving, the liver is subjected to axial static indentation tests in which the same tests are performed on different faces of a bovine liver piece. The results of each axes are compared. Another comparison is done in order to see the effect testing condition on the soft biological tissue; the test data gathered from the liver stored in the serum liquid and the liver kept bare is compared.

The inverse finite element method is a numerical approach in which an optimization algorithm is coupled with a finite element analysis in order to find the optimum coefficients of the material model defined in the finite element model. The finite element model is the simulation of the experimental process in which the physical and mechanical properties of the experimented material are assigned and the mechanical response of the material is obtained. In our model, the material is constructed as isotropic and nonlinear hyperelastic and linear viscoelastic. The FE data is pass on to the optimization procedure in which the nonlinear least squares method is used.

To conclude, all the results found by any method mentioned above are presented with comparisons. The results belonging to the synthetic material showed that it is mechanically similar to a soft biological tissue in terms of nonlinearity and viscoelasticity but, it's not in a similar range with the bovine liver. The keeping condition of the liver is also seen to make a sense becuase the data obtained from the liver kept in serum liquid gave a different force range with a more smooth data. The inverse FE method is run for the Yeoh hyperelastic material model and lineer viscoelastic model and by this way, the coefficients of the materials used in this study are provided for soft tissue simulations.

YUMUŞAK DOKULARIN MALZEME KATSAYILARININ DENEYSEL VERİLER VE TERSİNE SONLU ELEMANLAR YÖNTEMİ KULLANILARAK HESAPLANMASI

ÖZET

Bu tezde, sığır karaciğeri ve sentetik bir malzeme üzerinde yapılan bir takım basma deneyleri sunulmuş ve deney verileri kullanılarak, tersine sonlu elemanlar metodu ile malzemelere ait malzeme katsayıları hesaplanmıştır.

Literatür, yumuşak biyolojik dokulara ait tespit edilmiş malzeme katsayılarına ihtiyaç olagelmiştir. Farklı yumuşak dokular için yayınlanmış değerler mevcuttur fakat, deney koşulları ve deney ortamı sonuçları etkiler. Çünkü yumuşak biyolojik dokular canlılığa, korunma koşullarına ya da sınır koşullarına göre değişen mekanik tepkiler gösterebilir. Ayrıca, doğu mekanik modeli saptamak da önemlidir zira, malzemeye atanmış malzeme modeline ait olan katsayılar hesaplanır. Öte yandan, sentetik malzeme, yumuşak biyolojik dokulara yakın mekanik özellikler göstermesi öngörüsüyle bu çalışmaya dahil edilmiştir. Yapay malzeme, simüle edilen yumuşak dokuyla benzer mekanik özellikler taşıdığı sürece, farklı deney şartları için deney datası sağlayarak simülasyon modellerinin doğrulanmasına katkı sağlar.

Bu çalışmada, hem Aquaflex Ultrasound Gel Pad isimli sentetik malzeme üzerinde hem de sığır karaciğeri üzerinde statik basma deneyleri ve gevşeme deneyleri yapılmıştır. Karaciğer deneyleri cansız ortamda gerçekleştirilmiştir. Deneylerden elde edilen veriler eğri oturtma ve tersine sonlu elemanlar yöntemleri ile çeşitli malzeme modellerine ait ksatsayıları bulmak üzere kullanılmıştır. Aquaflex Ultrasound Gel malzemesi için, statik basma deney verileri Mooney-Rivlin ve Yeoh tipi malzeme modellerine oturtulmuş ve katsayılar elde edilmiştir. Gevşeme deneyleri verileri ise gevşeme fonksiyonu için kullanılan Prony seri açılımına oturtulmuştur. Her iki tip tersine sonlu elamanlar yönteminde de katsayı tespit etmek üzere kullanılmıştır. Bu amaçla, malzeme ve deneyi simüle eden sonu elemanlar modelleri bir sonlu elemanlar yazılımı aracılığıyla her durum için oluşturulmuştur. Bütün bu işlemler sığır karaciğeri deneylerinden elde edilen verilere de

uygulanmıştır. Mekanik davranış bakımından eksenel farklılıkları tespit etmek amacıyla, bir karaciğer parçasının farklı eksenlerdeki yüzlerinde aynı basma deneyini tekrarlanmış ve sonuçlar kıyaslanmıştır. Başka bir karşılaştırma da, karaciğerin saklanma koşullarının veriye yansımasını görmek amacıyla, deney öncesi serum içince saklanan ve saklanmayan dokularda yapılan deneylerin sonuçlarına bakılarak yapılmıştır.

Tersine sonlu elemanlar yöntemi, doğru katsayıları bulmak amacıyla bir en iyileme algoritması ile malzemenin model içinde tanımlandığı bir sonlu elemanlar analizinin birlikte çalıştırıldığı sayısal bir yaklaşımdır. Sonlu elemanlar modelinde malzemenin fiziksel ve mekanik özellikleri girilir ve malzemenin simülasyon sonundaki mekanik cevabı elde edilir. Bu çalışmadaki modelde malzeme izotropik, doğrusal olmayan hiperelastik ve doğrusal vizkoelastik olarak tanımlanmıştır. Sonlu elemanlar analizinden elde edilen veriler ise doğrusal olmayan en küçük kareler yönteminin çalıştırıldığı en iyileme sürecine katılır.

Sonuç olarak, yukarıda bahsi geçen tüm metodlarla elde edilen tüm veriler çalışmada sunulmuştur. Sentetik malzemeden elde edilen veriler, bu malzemenin, doğusal olmayan ve vizkoelastik davranış sergilemesi bakımından yumuşak biyolojik dokulara benzerliğini ortaya koymuş ancak, sonuçların sığır karaciğerinden elde edilenler ile aynı aralık civarında olmadığı görülmüştür. Yumuşak dokuyu saklama koşullarının etkin olduğu sonucuna varılmıştır, zira, serum sıvısı içinde korunmuş karaciğerden elde edilen veri aralığının farklı olduğu ve bu koşulun daha düzgün eğriler verdiği görülmüştür. Tersine sonlu elemanlar yöntemi, Yeoh hiperelastik malzeme modeli ve lineer vizkoelastik malzeme modeli için çalıştırılmış ve sonraki simülasyonlarda da kullanılabilecek katsayılar sunulmuştur.

1. INTRODUCTION

1.1 Purpose of the Thesis

The main objective of this thesis is the determining the material parameters of soft biological tissues by using appropriate material models in order to allow realistic force response in material model simulations.

Modeling deformation behavior of soft tissues under known boundary conditions and forces is a fruitful research area of engineering and biomedical that finds place in various applications such as virtual surgery, blood flow simulations, implant operations, etc. Accurate modeling of the deformation behavior is strictly related to the mathematical power of the proposed model and accurate determination of the coefficients that are used in the material model to project its characteristics.

For this reason, it is aimed in this study, that a specific soft tissue bovine liver, has been subjected to a series of experiments and its material coefficients have been computed via Inverse Finite Element Method. On the way of this work, it has been observed that precise validation of these material models was also a challange and required further study. Therefore, not only bovine liver but also a synthetic, soft tissue-like material which was predicted to be so, was used in order to discover its deformation behavior and obtain its material coefficients. Laboratory experiments which are performed on synthetic materials will contribute to the development of some physical standarts for the verification process of the proposed models, when isotropy and homogeneity of the synthetic materials and the advantage to be able to repeat the experiments under constant conditions are considered.

1.2 Literature Review

There are various methods such as finite element, spring-mass systems, and particle-based systems in order to model the deformation behaviours of soft tissues under physical conditions. The precise determination of material coefficients is of great importance in modelling. Literature of biomechanics or of similar areas contains many studies about the parameter determination of soft tissues but, each of them differs in some way that the parameters found strictly depend on that specific work's conditions. Some differ by the method and assumptions used to model the material behaviour, some differ by the chosen material model, some differ in the subject soft tissue on which the material tests are conducted, and some differ by the experimental environments. Real time modelling applications such as virtual surgery simulators can cause mislearning because of wrong material coefficients. Since coefficient determination depends on material tests, testing environment and conditions should be taken into consideration as well as the methods used to determine the material coefficients

The first step for the determination of material coefficients of any material is performing material tests; these tests can vary as uniaxial, biaxial, tension or compression tests and more, which will show the deformation characteristics of the material. In order to find out the coefficients of tissues of living things, numerous experiments have been conducted on different organs in different conditions. Some were performed *in vivo,* which literally means 'in life', and is a way of experimentation using a whole, living organism in its natural environment. Some were performed *ex vivo,* which literally means 'out of the living'. Ex vivo refers to experimentation or measurements done in or on tissue in an artificial environment outside the organism with the minimum alteration of natural conditions. Ex vivo conditions allow experimentation under more controlled conditions than possible in the intact organism. Another experimentation technique is *in vitro* experimentation, which means doing the tests on the living organism but in the artificial laboratory conditions. Also, there are examples of soft tissue researchers who have established their own environments to enhance the quality of the measurements as will be described below.

The first in vivo indentation experiments conducted on human liver were done by Carter [1] in 1999. Carter et al. performed several indentation tests both on human

liver in vivo and on swine liver and spleen ex vivo. All the results demonstrated highly nonlinear stress-strain behaviour. Swine spleen was compared to swine liver which was found to be stiffer. The mean elastic modulus for the right lobe of human liver was found about 0.27 MPa with one exceptional case of a diseased liver with an elastic modulus of 0.74 MPa. It was shown in the paper that an exponential stress-strain law could accurately fit the uniform stress test data [1].

A wide range of experiments are performed on animal organs of which tissues are assumed to be closely similar to that of humans. Kim and Srinivasan did in vivo experiments on swine liver and kidney and analyzed the data by inverse finite element method in order to model the quasilinear viscoelastic and hyperelastic behaviour [2].

While in vivo tests are difficult to perform, ex vivo tests are known to give unrealistic data due to the death of the organ which results changes in the structure and mechanical behaviour despite the easier setup of the experiments. Kerdok [3] designed a special mechanism that maintains an in vivo-like environment for a nonliving organ outside the animal body. In order to preserve the viscoelastic behaviour which is thought to be induced by the blood perfusion system, Kerdok made the mechanism so as to simulate the surface humidity, inner body temperature and blood circulation [3]. This experimental setup and results were later used in another work that explores the effects of perfusion provided in laboratory environment.

The investigation was made by Ottensmeyer et al. [4] in 2004, to present the effects of testing environment on the viscoelastic properties of soft tissues. It is declared in that paper that mechanical properties of biological tissues change outside the living body, due to the alterations in both the physical and environmental conditions. However, most of the biological data in the literature have been acquired from ex vivo tests which can be conducted more easily [4]. The study compares the results of the tests conducted on liver in four different conditions: in vivo, ex vivo with a perfusion mechanism, ex vivo unperfused, and untreated. It is found that the data showed >50% differences in steady state stiffness between the in vivo and ex vivo unperfused conditions, this difference decreased to 17% between in vivo and ex vivo perfused conditions. Variations were also detected in the time domain and frequency domain responses for all testing conditions [4].

There is also one study in this area on the validation side of soft tissue models. Kerdok et al. [5] aimed to find a better way of validation due to the intrinsic limitations of FEM models by making up a database of relevant information so as to be used for validation of real-time soft tissue deformation. Teflon beads were embedded with an exact pattern into a simple 8 cm silicone rubber cube and this cube was subjected to uniaxial compression tests while CT images were taken and experimental results were also compared to the results of finite element computations. Truth cube project was the first in this area; a synthetic material was first used for validation soft tissue simulations, the constructed cube had been resulted in a structure with a modulus of elasticity in the range of soft biological tissues [5]. However, viscoelasticity, which is one of the most distinguishing properties of soft tissues and which is the biggest challenge for soft tissue experiments, was not present in the truth cube.

As mentioned before, the material coefficients are searched to be used in deformation behaviour simulations, and there have been modelling studies either including parameter detection or alone. Dogan and Celebi presented their work on real-time deformation simulation of non-linear viscoelastic soft tissues using the existing material parameters in literature [6]. A new hybrid method was proposed and the results of deformation simulation of viscoelastic soft tissue were compared to the linear approach and it was deduced that the outcome of the deformation simulation of a human liver based on nonlinear QLV was more accurate and convenient than that of the linear approach [6].

1.3 Scope of the Present Work

This thesis can be divided into two main parts: material testing of an artificial material and liver, and computation of material parameters for both materials and additionally it includes s brief information about the continuum mechanics on which the soft tissue material models are based.

The aim of the study, the outline of the thesis and literature review are given in the first chapter. The second chapter makes the introduction to the continuum mechanics giving the fundemental information about the concept of continuum, motion description, stress and strain components. Mechanical properties of soft biological tissues are also summarized in this chapter, by giving basic information about stress-

strain relationship and viscoelasticity of soft tissues. Lastly, mathematical models, classified as hyperelasticity and viscoelasticity models, are explained in the chapter.

In the third chapter, after a brief information about material testing, details of our experimental setup and the materials used in this study are described. The experiments, conducted on both artificial gel pad and liver and grouped as static indentation and ramp-hold tests, are presented graphically.

Fourth chapter explains our finite element model built to simulate the material tests. Contact model is seperately discussed as it is the main part of such compression simulations constructed via finite element tools.

Fifth chapter is about the computation part of the thesis since the inverse finite element method is explained in this chapter; inverse finite element algorithm is described and the optimization methods used in the inverse FE method are represented. Mainly, three optimization algorithms are taken into consideration: Gauss-Newton, Levenberg-Marquardt, and trust region methods.

Sixth chapter is the last chapter and in this chapter all the results obtained from the inverse FE computations are presented and the results, including the experimental data are discussed.

2. CONTINUUM MECHANICS FOR SOFT TISSUES

2.1 Fundamentals of Continuum Mechanics

Physical objects of the real world consist of molecules of atomic and subatomic particles. This microscopic system of the objects can be investigated in atomic levels in order to understand some physical phenomena that take part in each micro structure. However, not every time the search in microscopic level is useful in engineering. Continuum mechanics is a method to analyse the pysical phenomena in macroscopic level without getting into the detailed molecular level structure of objects and by generalizing the properties by gathering the effects of micro structures as much as possible. Therefore, it is an approximation in which a few quantities that are small enough to present the microstructural effects show the averages over dimensions and the continuum theory can be applied to all materials regardless of the microstructures included [7].

The scope of continuum mechanics can be summarized as

- Kinematics (motion and deformation),
- Stress in a continuum and
- The mathematical description of the motion of a continuum [7].

In order to build the physical laws of continuum mechanics mathematically, it is essential to comprehend the basic concepts related to motion, deformation and stress in a continuum.

A continuum body or shortly continuum, is the body of an object in which the discrete structure of molecules, the gaps between the molecules are ignored and the body is assumed continuous or piecewise continuous by a zoomed out view. Although a continuum body is said to represent a continuous structure, it is actually composed of continuum particles. The term *continuum particle* doesn't refer to a particle in the atomic level and is not related to the point mass of Newtonian mechanics.

It is the tiniest continuum part of the continuum body which reflects the collective behavior of the microstructures that it consists of and on which the rules of continuum mechanics work. The mass and volume of a continuum is also considered continuous (or piecewise continuous) [7].

2.1.1 Motion Description

The configuration of the displacement of a continuum particle is shown in Figure 2.1. Let Γ_0 be the boundary of the undeformed body Ω_0 and Γ be the boundary of the deformed body Ω.

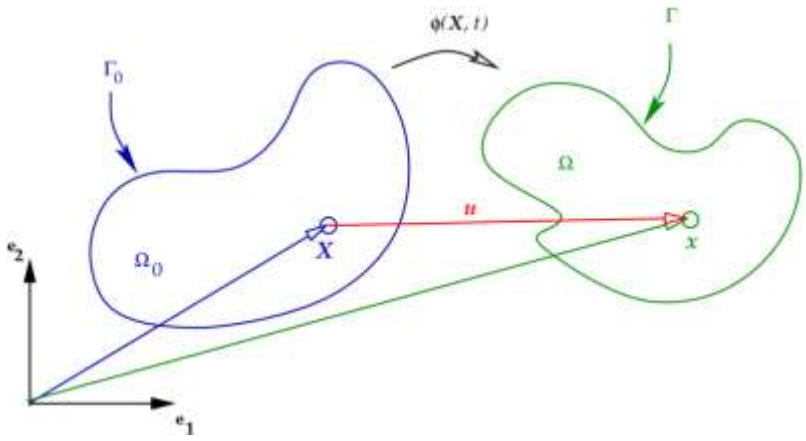

Figure 2.1 : The configuration of the deformed and undeformed positions of a continuum [23].

The position vector of an arbitrary point on a continuum before displacement is defined by the vector $\boldsymbol{X} = [X_1\ X_2\ X_3]^T$ and the position vector of that point after displacement is defined by the vector $\boldsymbol{x} = [x_1\ x_2\ x_3]^T$. The positions before and after displacement has such a relationship that

$$\boldsymbol{x} = \boldsymbol{X} + \boldsymbol{u} \qquad \textbf{(2.1)}$$

where $\boldsymbol{u} = [u_1\ u_2\ u_3]^T$ is the displacement vector and all three vectors are in the same global coordinate system and this motion is defined by the function $\Phi(X, t)$.

The coordinates of the undeformed state, $\boldsymbol{X}$, is called the Lagrangian coordinates whereas the coordinates of the deformed state, $\boldsymbol{x}$, is called the Eulerian coordinates. Even though, both set of coordinates can be used in kinematic or dynamic equations,

Lagrangian description is preferred for solid mechanics because the deformation history is meaningful in solid kinematics [8].

In order to define the basic strain variables of the continuum mechanics, the deformation on the length of a line element is used. For that element, if the deformation is known that is, when the change of the distance between any two points on the line element is known, change in volume or area for that element can also be calculated. A differential line element notated as above can be expressed as

$$d\boldsymbol{x} = \frac{\partial \boldsymbol{x}}{\partial \boldsymbol{X}} d\boldsymbol{X} = \boldsymbol{J} d\boldsymbol{X} \tag{2.2}$$

by means of the *matrix of position vector gradients*, also called the *Jacobian matrix*. The expansion of $\boldsymbol{J}$ is as follows:

$$\boldsymbol{J} = \frac{\partial \boldsymbol{x}}{\partial \boldsymbol{X}} = \begin{bmatrix} \frac{\partial x_1}{\partial X_1} & \frac{\partial x_1}{\partial X_2} & \frac{\partial x_1}{\partial X_3} \\ \frac{\partial x_2}{\partial X_1} & \frac{\partial x_2}{\partial X_2} & \frac{\partial x_2}{\partial X_3} \\ \frac{\partial x_3}{\partial X_1} & \frac{\partial x_3}{\partial X_2} & \frac{\partial x_3}{\partial X_3} \end{bmatrix} = [x_{X_1} \; x_{X_2} \; x_{X_3}] \tag{2.3}$$

When there are no displacements in all three dimensions, $\boldsymbol{J}$ becomes identity matrix with a positive determinant that is equal to 1 and then $d\boldsymbol{x}$ equals $d\boldsymbol{X}$.

A physically possible continuous deformation is necessarily and sufficiently provided by the condition that the Jacobian is positive definite, that is the determinant of the Jacobian is greater than zero. This condition should be valid for the transformation from the reference configuration to the current configuration too. In the case in which this condition is provided on every particle of the material body, the transformation from the Eulerian description to the Lagrangian description or vice versa is possible [8].

2.1.2 Strain Components

Strain is the change of length of a body and its components are derived from the elongation of the line element. If the original length of the element is defined as l_o

and the deformed length is defined as l_d, the following equalities can be written using the squares of the defined lengths.

$$(l_o)^2 = d\boldsymbol{X}^T d\boldsymbol{X} \tag{2.4}$$

$$(l_d)^2 = d\boldsymbol{x}^T d\boldsymbol{x} = d\boldsymbol{X}^T \boldsymbol{J}^T \boldsymbol{J} d\boldsymbol{X} \tag{2.5}$$

$$(l_d)^2 - (l_o)^2 = d\boldsymbol{X}^T \boldsymbol{J}^T \boldsymbol{J} d\boldsymbol{X} - d\boldsymbol{X}^T d\boldsymbol{X} = d\boldsymbol{X}^T (\boldsymbol{J}^T \boldsymbol{J} - \boldsymbol{I}) d\boldsymbol{X} \tag{2.6}$$

Equation 2.6 can be rewritten by substituting the *Green-Lagrange strain tensor*, ε as below:

$$\boldsymbol{\varepsilon} = \frac{1}{2}(\boldsymbol{J}^T \boldsymbol{J} - \boldsymbol{I}) \tag{2.7}$$

$$(l_d)^2 - (l_o)^2 = 2 d\boldsymbol{X}^T \boldsymbol{\varepsilon} d\boldsymbol{X} \tag{2.8}$$

As we now the expansion of the Jacobian, the Green-Lagrange strain tensor can be written explicitly by means of gradient vectors x_{X_i} as follows:

$$\boldsymbol{\varepsilon} = \frac{1}{2}\begin{bmatrix} (x_{X_1}^T x_{X_1} - 1) & x_{X_1}^T x_{X_2} & x_{X_1}^T x_{X_3} \\ x_{X_1}^T x_{X_2} & (x_{X_2}^T x_{X_2} - 1) & x_{X_2}^T x_{X_3} \\ x_{X_1}^T x_{X_3} & x_{X_2}^T x_{X_3} & (x_{X_3}^T x_{X_3} - 1) \end{bmatrix} \tag{2.9}$$

In order to rewrite the strain tensor in terms of the displacement vector gradient, $\boldsymbol{J}_d$, the relation $\boldsymbol{J} = \boldsymbol{J}_d + \boldsymbol{I}$ is substituted and the following expression is obtained:

$$\varepsilon_{ij} = \frac{1}{2}\left(u_{i,j} + u_{j,i} + \sum_{k=1}^{3} u_{k,i} u_{k,j}\right), \quad i, j = 1, 2, 3 \tag{2.10}$$

where ε_{ij} are the elements of the tensor ε and $u_{i,j} = \partial u_i / \partial X_j$ $(i, j = 1, 2, 3)$. Equations 2.9 and 2.10 clearly show that the Green-Lagrange strain components are nonlinear.

The strain tensor is obviously symmetric (Equation 2.9), thus the following six independant components of the tensor can be written as a vector as follows:

$$\boldsymbol{\varepsilon}_v = [\varepsilon_{11}\ \varepsilon_{22}\ \varepsilon_{33}\ \varepsilon_{12}\ \varepsilon_{13}\ \varepsilon_{23}]^T \quad \textbf{(2.11)}$$

Here, ε_{ij} is called *normal strains* when $i = j$ and called *shear strains* when $i \neq j$. Because the gradient vectors x_{X_i} define the rate of change along the direction X_i, normal strains are the elements that reflects the length change along the axes; shear strains are the measures of the change of the relative orientation between axes.

There are other simplified calculation methods of strain components. For simple cases, the geometric interpretation is formed as follows and it is called *engineering strain* or *Cauchy strain*.

$$\varepsilon = \frac{(l_d - l_o)}{l_o} \quad \textbf{(2.12)}$$

Natural or *Logarithmic strain* is defined as $l_d = (1+\varepsilon)l_o$. Another definition related to strain is *stretch ratio*. It is the measure of the extensional or normal strain of a differential line element, which can be defined at either the undeformed configuration or the deformed configuration. Denoted by Λ, the stretch ratio is defined as l_d / l_o.

2.1.2.1 Right and Left Cauchy-Green Deformation Tensors

Alternative to the Lagrangian and Eulerian strain tensors, there are other deformation expressions that are invariant under a rigid-body motion. Right Cauchy-Green deformation tensor and left Cauchy-Green deformation tensor are some of these.

Right Cauchy-Green tensor, which is in literature generally referred to as Green deformation tensor [7], is defined as

$$\boldsymbol{C}_r = \boldsymbol{J}^T\boldsymbol{J}\ , \quad \textbf{(2.13)}$$

and left Caucy-Green tensor is defined as

$$\boldsymbol{C}_l = \boldsymbol{J}\boldsymbol{J}^T\ . \quad \textbf{(2.14)}$$

Equation 2.7 can be rewritten in terms of Green deformation tensor, since they have a linear relationship. Similarly, Eularian description can be rewritten in terms of right Cauchy-Green deformation tensor.

$$\boldsymbol{\varepsilon} = \frac{1}{2}(\boldsymbol{C}_r - \boldsymbol{I}) \tag{2.15}$$

2.1.3 Principal Strains and Strain Invariants

Principal directions of the strain tensor ε can be obtained by an eigenvalue problem.

$$(\boldsymbol{\varepsilon} - \lambda \boldsymbol{I})\boldsymbol{Y} = 0 \tag{2.16}$$

where λ is the eigenvalue and $\boldsymbol{Y}$ is the eigenvector of the matrix $\boldsymbol{\varepsilon}$.

Equation 2.16 is solved by equalizing the determinant $|\boldsymbol{\varepsilon} - \lambda \boldsymbol{I}|$ to 0. Since the strain tensor is symmetric, the equation has three real roots, λ_1, λ_2, and λ_3, in three dimensional case.

$$(\varepsilon - \lambda_i I)Y_i = 0, \quad i = 1,2,3 \tag{2.17}$$

Considering that the eigenvectors Y_i are orthogonal unit vectors, Equation 2.17 yields to the following solution:

$$Y_i^T \boldsymbol{\varepsilon} Y_i = \lambda_i, \quad i = 1,2,3 \tag{2.18}$$

$$\boldsymbol{Y}^T \boldsymbol{\varepsilon} \boldsymbol{Y} = \begin{bmatrix} \lambda & 0 & 0 \\ 0 & \lambda & 0 \\ 0 & 0 & \lambda \end{bmatrix} \tag{2.19}$$

Y_i are called the principal directions and λ_i are called the principal normal strains.

The following definitions are used the constitutive equations of continuum mechanics and are called the *principal strain invariants*.

$$\begin{aligned} I_1 &= tr(\boldsymbol{\varepsilon}), \\ I_2 &= \frac{1}{2}\left\{(tr(\boldsymbol{\varepsilon}))^2 - tr(\boldsymbol{\varepsilon}^2)\right\}, , \\ I_3 &= \det(\boldsymbol{\varepsilon}) = |\boldsymbol{\varepsilon}| \end{aligned} \tag{2.20}$$

For the case of symmetric strain tensor, the invariants are

$$\begin{aligned} I_1 &= \lambda_1 + \lambda_2 + \lambda_3, \\ I_2 &= \lambda_1\lambda_2 + \lambda_1\lambda_3 + \lambda_2\lambda_3, \\ I_3 &= \lambda_1\lambda_2\lambda_3. \end{aligned} \qquad \textbf{(2.21)}$$

2.1.4 Stress and Stress Components

Stress is the measure of pressure in the theory of continuum mechanics and it is related to the strenght of the material, since it indicates the magnitude of the internal forces the material can sustain [9].

Beyond the limits of the material's strength, stress can lead to a permanent shape change or a physical failure on the material. For a continuum body with a cross-sectional area of A, if the force that acts into the body is F, then stress, σ, is calculated as

$$\sigma = F/A. \qquad \textbf{(2.22)}$$

The dimension of stress is the same with that of pressure and the unit stress is Pascal (Pa), which is $1N/m^2$, in the International System of Units.

The equalibrium of forces acting on a continuum body is considered to obtain the stress formulations in continuum mechanics.

Let's consider a deformable continuum body shown in Figure 2.2.

Here in Figure 2.2, t is the force measured per unit surface area for the deformed configuration and is called the Cauchy (true) traction vector, $\boldsymbol{ds}$ is the unit surface area, and $\boldsymbol{n}$ is the normal vector of surface $\boldsymbol{S}$. The capitalized notations represent the same values for the undeformed configuration. $\boldsymbol{T}$ is called the first Piola-Kirchhoff (nominal) traction vector.

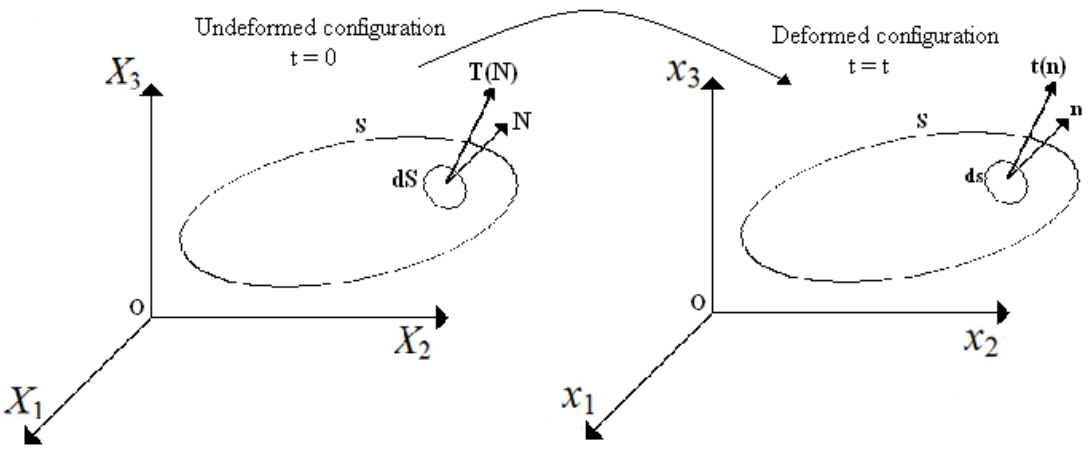

Figure 2.2 : Traction forces acting on infinitesimal surface elements with outward unit normals.

Using these notations, the following equation can be written for every infinitesimal surface element:

$$df = \boldsymbol{t}ds = \boldsymbol{T}dS \,. \qquad \textbf{(2.23)}$$

According to the *Cauchy's Stress Theorem*, there exist unique second-order tensor fields σ and P so that

$$\begin{aligned} &\boldsymbol{t}(\boldsymbol{x},t,\boldsymbol{n}) = \boldsymbol{\sigma}(\boldsymbol{x},t)\boldsymbol{n} \quad \text{or} \quad t_a = \sigma_{ab} n_b, \\ &\boldsymbol{T}(\boldsymbol{X},t,\boldsymbol{N}) = \boldsymbol{P}(\boldsymbol{X},t)\boldsymbol{N} \quad \text{or} \quad T_{AB} = P_{AB} N_B \end{aligned} \,. \qquad \textbf{(2.24)}$$

where σ is a symmetric tensor called the *Cauchy (true) stress tensor* (simply the *Cauchy stress*) and P is called the *first Piola-Kirchhoff (nominal) stress tensor* (simply the *Piola stress*) [7]. Cauchy stress can also be written in matrix form.

$$\boldsymbol{\sigma} = \begin{bmatrix} \sigma_{11} & \sigma_{12} & \sigma_{13} \\ \sigma_{21} & \sigma_{22} & \sigma_{23} \\ \sigma_{31} & \sigma_{32} & \sigma_{33} \end{bmatrix}. \qquad \textbf{(2.25)}$$

The elements of this matrix, σ_{ab} is called the *stress components* of the Cauchy stress tensor. Since the Cauchy stress tensor is symmetric, $\sigma_{12} = \sigma_{21}, \sigma_{13} = \sigma_{31}, \sigma_{23} = \sigma_{32}$.

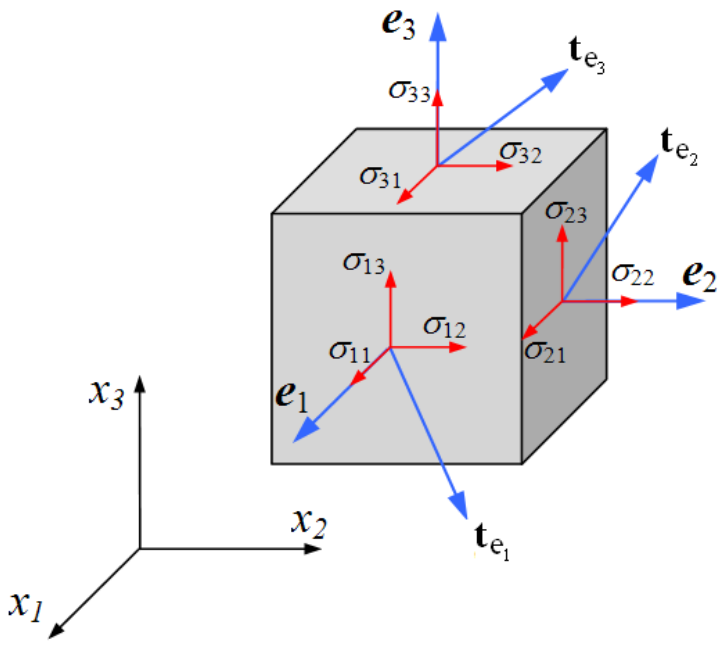

Figure 2.3 : Positive stress components of the traction vectors acting on the faces of a cube [24].

2.2 Mechanical Properties of Soft Biological Tissues

Soft biological tissues have complex inhomogeneous structures, thus they show complex mechanical behaviors which can be summarized as nonlinearity, anisotropy and viscoelasticity. The stress-strain relation of most soft biological tissues are nonlinear. When the mechanical properties change axially, this is called anisotropy and soft biological tissues are anisotropic structures. Water and other fluid that they contain give them viscosity and thus, soft biological tissues show viscoelastic behavior which is a time-dependant property and which also depends on vitality and perfusion of the tissue. Also, soft biological tissues are considered as incompressible.

These mechanical properties is explained in details in the subsequent sections.

2.2.1 Stress - Strain Relation of Soft Biological Tissues

The stress-strain relation which shows a material's mechanical properties have been found as nonlinear for soft biological tissues according to the materials tests performed up to now. Nonlinearity of the stress-strain relation is a general characteristic of all soft tissues.

However, as each soft tissue has its specific relation, this relation also depends on the location of the tissue on which the tests are conducted. That is, the mechanical properties of one tissue also varies within the tissue and should not be handled as homogeneous. Also because of anisotropic structure, the stress-strain relation differs for loading to each axis.

It has been experimentally found that for most materials, the measured strains are proportional to the applied forces, provided that the load doesn't exceed the elastic limit which causes the destruction of the material. This experimental observation states that the stress components at any point in the body are a linear function of the strain components. This relationship between stress and strain, called the generealization of the Hooke's law: $\boldsymbol{\sigma = E\varepsilon}$. It doesn't apply to viscoelastic, plastic, or viscoplastic materials. Hooke's law is explained in details under Section 2.3.1.

If the case is the nonlinear relation between stress and strain, then Hooke's law fail again. The strains are, for this case, not a linear function of the stresses but a nonlinear function. And if the work done by the stresses is independent of the deformation path, the relationship is expressed as a function of this stored energy, which is the strain energy density function for hyperelastic materials.

The following figure summarizes the formulation of the stress-strain relationship with respect to the linearity of the relation, where $f(\boldsymbol{\varepsilon})$ in Figure 2.4 is an undetermined non-linear function.

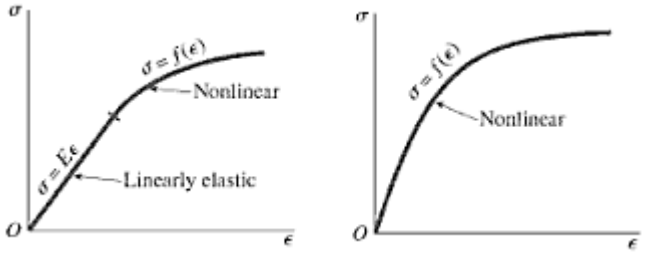

Figure 2.4 : Types of idealized material behaviour. On the left is the elastic nonlinear stress-strain curve and on the right is the general nonlinear stress-strain curve [25].

2.2.2 Viscoelasticity of Soft Biological Tissues

Viscoelasticity is a property of a material exhibiting both elasticity and viscosity when it is deformed. Elastic materials strain instantaneously when they're stretched or compressed and when the stress is removed, they return to their original shape. On the other hand, viscosity is a measure of resistance of fluids to deformation caused by a shear or tensile stress.

There are some phenomena that are seen in viscolastic materials and some definitions are made on these phenomena. When a material body is suddenly strained and the strain is held constant, the stress applied into the body, that causes the deformation, gradually decrease to a limit value. This behavior is called *stress relaxation* (simply *relaxation*). If a sudden stress is induced into the body and held constant for some time, it is measured that the body continues to deform. This behavior is called *creep.* Another feature is *hysteresis*. If the body is subjected to cyclic loading, the stress-strain relation that is recorded during loading differs from the relation in the unloading process. An amount of energy loss is observed between the stress-strain curves of the loading and unloading processes at each cycle. Relaxation, creep and hysteresis are features of viscoelastic materials and these features reflects the time dependancy of deformation of viscolelastic materials in contrast with elastic materials.

Different mechanical models have been developed to reflect the viscoelastic properties of materials in constitutive equations. Where elastisity is modeled by linear springs in order to produce an instantaneous deformation proportional to the load, viscosity is modeled by dashpots in order to produce a velocity proportional to the load at any instant. Three basic mechanical models of viscoelastisity, composed of linear springs with spring constant k and dashpots with viscosity coefficient λ, are presented by Maxwell, Voigt and Kelvin (Figure 2.5).

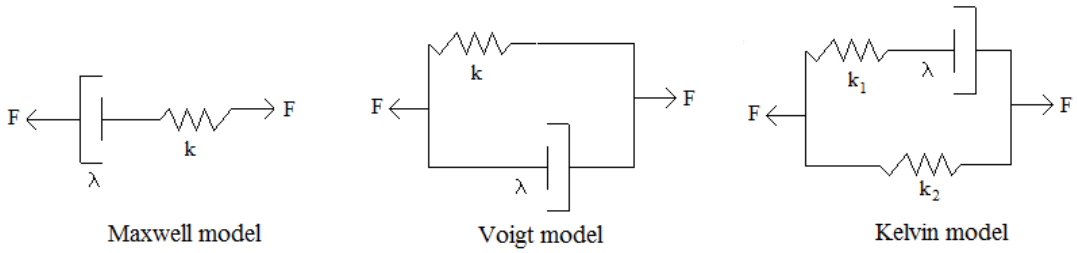

Figure 2.5 : Mechanical models for a viscoelastic material: Maxwell model, Voigt model and Kelvin model (also called *a standart linear solid*) (The image is re-generated from a picture in [26]).

If F is the force applied to the linear spring and caused an elongation of u, then $F = ku$. If F is applied on a system with a dashpot and produced a deflection velocity $\dot{u}$, then $F = \lambda \dot{u}$.

In Maxwell model, the force is transmitted from the spring to the dashpot and the system is modeled as below:

$$\dot{u} = \frac{\dot{F}}{k} + \frac{F}{\lambda} \qquad \textbf{(2.26)}$$

If the force is suddenly applied, the spring will react but the initial deflection of the dashpot will be zero because dashpots deforms in time; thus the following initial condition will be valid for the case at $t = 0$.

$$u_0 = \frac{F_0}{k} \qquad \textbf{(2.27)}$$

In Voigt model, the spring and the dashpot have the same displacement; they share the force applied to the system. Voigt model can be written as below:

$$F = ku + \lambda \dot{u} \qquad \textbf{(2.28)}$$

A sudden loading will create no displacement because the reaction of the spring is dependant to the dashpot and the displacement of the dashpot at $t = 0$ is zero. The initial condition will be as follows:

$$u_0 = 0 \qquad \textbf{(2.29)}$$

In Kelvin model, there is a parallel connection between a linear spring and system that is composed of a spring and dashpot connected serially. If the previous approach

used for Maxwell and Voigt models is applied, the following equation is obtained for Kelvin model:

$$F + \frac{\lambda}{k_1}\dot{F} = k_2\left(u + \frac{\lambda}{k_2}\left(1 + \frac{k_2}{k_1}\right)\dot{u}\right) \qquad \textbf{(2.30)}$$

The sudden loading case with the applied force F_0 and the displacement u_0 gives the following initial condition:

$$\frac{\lambda}{k_1}F_0 = \lambda\left(1 + \frac{k_2}{k_1}\right)u_0 \qquad \textbf{(2.31)}$$

The term $\frac{\lambda}{k_1} = \tau_\varepsilon$ is called the *relaxation time for constant strain* and the term $\frac{\lambda}{k_2}\left(1 + \frac{k_2}{k_1}\right) = \tau_\sigma$ is called the *relaxation time for constant stress.*

If the equations 2.26, 2.28 and 2.30 are solved seperately for the deformation, the creeping behavior of a material, which presents the elongation produced by a sudden loading of a constant force, are found. Creep functions are given in the following equations 2.32, 2.33 and 2.34 respectively for Maxwell, Voigt and standart linear solid (Kelvin) models.

$$c(t) = \left(\frac{1}{k} + \frac{1}{\lambda}t\right)1(t) \qquad \textbf{(2.32)}$$

$$c(t) = \frac{1}{k}(1 - e^{-(k/\lambda)t})1(t) \qquad \textbf{(2.33)}$$

$$c(t) = \frac{1}{k_2}\left[1 - \left(1 - \frac{\tau_\varepsilon}{\tau_\sigma}\right)e^{-t/\tau_\sigma}\right]1(t) \qquad \textbf{(2.34)}$$

Here, the solutions are based on the assumption that $F(t)$ is a unit-step function $1(t)$ and $1(t)$ is defined as

$$1(t)=\begin{cases} 0 & \text{if} \quad t<0, \\ 1/2 & \text{if} \quad t=0, \\ 1 & \text{if} \quad t>0. \end{cases} \tag{2.35}$$

Solving the equations 2.26, 2.28 and 2.30 for the force applied and assuming the deformation $u(t)=1(t)$, relaxation functions are obtained. Relaxation functions give us the force to be applied in order to save the unit elongation of the suddenly deformed material. The following equations 2.36, 2.37 and 2.38 are the relaxation functions $g(t)$, for Maxwell, Voigt and standart linear solid (Kelvin) models respectively:

$$g(t)=ke^{-(k/\lambda)t}1(t) \tag{2.36}$$

$$g(t)=\lambda\delta(t)+k1(t), \qquad \delta(t)=\begin{cases} \delta(t)=0 \quad \text{for } t<0 \text{ and } t>0, \\ \int_{-\varepsilon}^{\varepsilon} f(t)\delta(t)dt=f(0) \quad \text{for } \varepsilon>0. \\ (f \text{ is an arbitrary function continuous at } t=0 \end{cases} \tag{2.37}$$

$$g(t)=\frac{1}{k_2}\left[1-\left(1-\frac{\tau_\sigma}{\tau_\varepsilon}\right)e^{-t/\tau_\varepsilon}\right]1(t) \tag{2.38}$$

The illustrations of creep and relaxation functions of these models are given in Figure 2.6 and Figure 2.7, respectively.

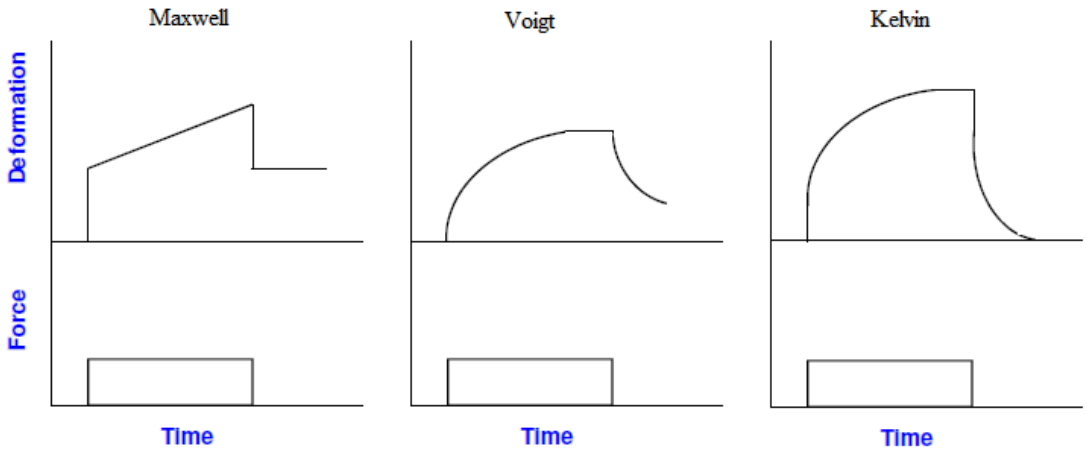

Figure 2.6 : Creep functions of Maxwell, Voigt and Kelvin models including the unloading phases [9].

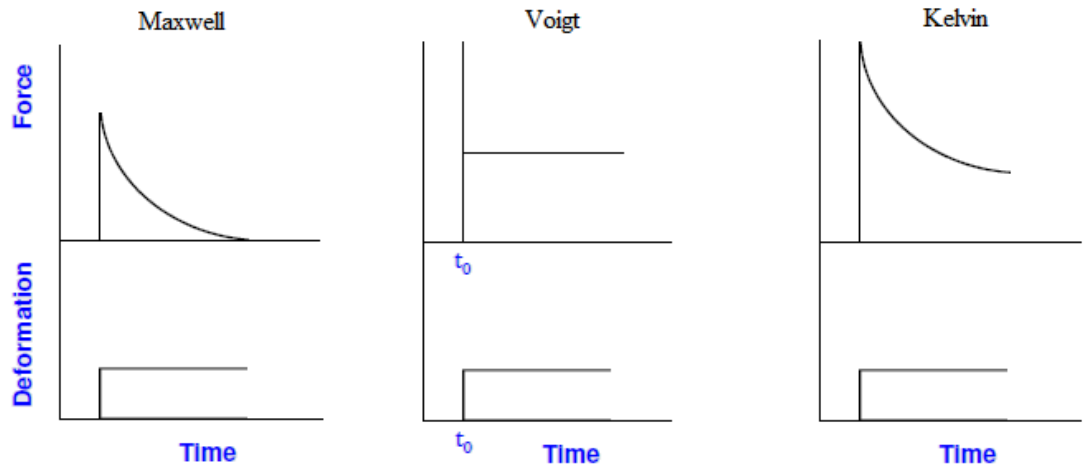

Figure 2.7 : Relaxation functions of Maxwell, Voigt and Kelvin models [9].

The illustrations reflects that for the Maxwell solid, sudden loading causes an immediate elongation by the linear elastic spring and the creep of the dashpot follows it (Figure 2.6). Sudden deformation produces an immediate reaction force and a decrease in force, that is stress relaxation, follows it (Figure 2.7).

For the Voigt model, the sudden loading doesn't produce an immediate deflection because the parallelly connected dashpot damps it; there occurs a gradual deflection where more of the force applied is taken by the spring (Figure 2.7).

For the Kelvin model, the relaxation function shows that the dashpot completely relaxes in time and the load remains constant as the effect of the spring which is characterized by the spring constant k_2 (Figure 2.7). Therefore, this constant is called the *relaxed elastic modulus.*

2.3 Mathematical Models of Soft Biological Tissues

Before explaining the mathematical models of soft biological tissues, constitutive equation concept should be known. An equation which describes a property of a material is called a constitutive equation of that material.When a piece of material is stretched by a force, stresses and strains develop at all points within the material. Stress–strain relationship is the constitutive relationship that describes the mechanical properties of a material, such as elasticity, plasticity, and linearity.

In order to be able to distinguish between different materials, the force-displacement relationship or equivalently the stress-strain relationship is required. To complete the specification of the mechanical properties of a material, additional set of equations , the constitutive equations, are needed. The form of the constitutive equations must be objective, and should not lead to change in the work and energy of the stresses under an arbitrary motion.

If the constitutive equations of a material depend only on the current state of deformation, th behavior is called *elastic*. Because elasticity is the property of a material to return to its original state after the load is removed. A special case of *Cauchy elastic materials*, in which the stress-strain relationship can be derived from the stored energy function (strain energy density function), and the material returns to its original state after the load is removed but linear elasticity do not describe this behavior, is termed *hyperelastic* or *Green elastic material*. Such materials have nonlinear stress-strain relationships but the work done by the stresses during deformation is path independent. Cauchy elastic materials are the ones for which the stresses cannot be derived from a stored energy function because the work done by the stresses depend on the path of the deformation. For *viscoelastic materials,* the work done by the stresses during deformation is path dependent due to the energy loss. The constitutive equations of viscoelastic materials are formulated in terms of rate of deformation measures in order to account for the energy loss.

Different material models have been developed based upon the constitutive equations mentioned above. Material models also vary for small deformation cases and large deformation cases and also compressibility makes sense in these models. Here in this section, the generalized Hooke's Law which is built to describe a general linear stress-strain relationship will be introduced, and while most of the material models used for soft biological tissues will be briefly mentioned, material models that are used in this study will be explained in details.

2.3.1 Generalized Hooke's Law

It has been found as the result of experiments that for most materials the measured strains are related to the applied forces. *Hooke's law* gives this relationship for the elastic materials, stating that the stress components at any point in the body are linear

function of the strain components. This law, shown in Equation 2.39 in vector and matrix notations, does not apply to viscoelastic, plastic, or viscoplastic materials [8].

$$\boldsymbol{\sigma}_v = \boldsymbol{E}_m \boldsymbol{\varepsilon}_v \tag{2.39}$$

Here, $\boldsymbol{\sigma}_v$, $\boldsymbol{\varepsilon}_v$, $\boldsymbol{E}_m$ are respectively, stress components, strain components, and matrix of elastic coefficients. In a case of a general material, the matrix of elastic components has 36 coefficients as in Equation 2.40 and each coefficient define the material elastic properties when the behavior is linear.

$$\boldsymbol{E}_m = \begin{bmatrix} e_{11} & e_{12} & e_{13} & e_{14} & e_{15} & e_{16} \\ e_{21} & e_{22} & e_{23} & e_{24} & e_{25} & e_{26} \\ e_{31} & e_{32} & e_{33} & e_{34} & e_{35} & e_{36} \\ e_{41} & e_{42} & e_{43} & e_{44} & e_{45} & e_{46} \\ e_{51} & e_{52} & e_{53} & e_{54} & e_{55} & e_{56} \\ e_{61} & e_{62} & e_{63} & e_{64} & e_{65} & e_{66} \end{bmatrix} \tag{2.40}$$

The number of independent coefficients change if the material exhibits special characteristics such as material symmetry, isotropy, orthotropy, or anisotropy. For the linearly elastic materials, the matrix is symmetric, therefore has 21 independent elements for the case of anisotropy. *Anisotropy* is a feature of a material to exhibit different mechanical properties in all 3 axes. For *orthotropic materials*, which show the same properties in two directions but show a different bahevior in the third direction, this number reduces to 9. If the material is *isotropic*, that is if the material's mechanical properties remain invariant independently from the loading axis, this number reduces to 2 and this two independent coefficients are denoted by λ and μ (Lame's constants). Below is the coefficient matrix for the homogeneous isotropic linearly elastic material.

$$\boldsymbol{E}_m = \begin{bmatrix} \lambda+2\mu & & & & & \\ \lambda & \lambda+2\mu & & \textit{symmetric} & & \\ \lambda & \lambda & \lambda+2\mu & & & \\ 0 & 0 & 0 & 2\mu & & \\ 0 & 0 & 0 & 0 & 2\mu & \\ 0 & 0 & 0 & 0 & 0 & 2\mu \end{bmatrix} \tag{2.41}$$

When the relationship between stress and strain is written explicitly using the Equation 2.39, the following equations are obtained.

$$\varepsilon_{ij} = \frac{1}{E}\left[(1+\gamma)\sigma_{ii} - \gamma(\sigma_{11}+\sigma_{22}+\sigma_{33})\right], \qquad i = 1,2,3$$
$$\varepsilon_{ij} = \left(\frac{1+\gamma}{E}\right)\sigma_{ij}, \qquad i \neq j \qquad \textbf{(2.42)}$$

Here, μ, E, and γ are, respectively, *shear modulus*, *Young's modulus(modulus of elasticity)*, and *Poisson's ratio*, where

$$\gamma = \frac{\lambda}{2(\lambda+\mu)} \quad \text{and} \quad E = 2\mu(1+\gamma). \qquad \textbf{(2.43)}$$

Poisson's ration cannot exceed 0.5. If the Poisson's ratio becomes close to 0.5, the elastic coefficient associated with the dillatation ($\sigma_{11}+\sigma_{22}+\sigma_{33}$) becomes very large and produces high stiffness that tends to resist any volume change.

2.3.2 Material Models For Large Deformations

Not all materials exhibit a linear deformation described as in the previous section. Due to the variety of material behaviors under deformation, various material models that cover nonlinearity and large deformation cases have been offered. Some of these material models are listed below.

- Neo-Hookean
- Mooney-Rivlin
- Yeoh
- Ogden
- Polynomial
- Arruda-Boyce

Neo-Hookean material model is the extension of Hooke's law for isotropic linear material to large deformation. Mooney-Rivlin model is a model used for the large deformation cases of nonlinear incompressible materials such as rubber. Yeoh model is for hyperelastic nearly incompressible materials too. For polymeric substances Arruda-Boyce model can be used. The material model that are used in this study are mooney-Rivlin and Yeoh models.

2.3.2.1 Mooney-Rivlin Material Model

Mooney-Rivlin material model describes the hyperlastic material behavior. The strain energy density function of this model, denoted by W, is written in the following form for the incompressible materials:

$$W = C_{10}(I_1 - 3) + C_{01}(I_2 - 3) \qquad \textbf{(2.44)}$$

I_1 and I_2 are strain invariants that are explained before, and C_{10} and C_{01} are material parameters having dimensions of stress but no direct physical interpretation. The incompressibility condition eliminates the third invariant from the equation, since $I_3 = J^2 = 1$ for incompressible materials and the term related to compressibility is $D_1(J-1)$.

This material model was built with the goal of finding a simple form of W that yields a nonlinear stress-strain relationship in extension but a linear behavior in shear [10].

This material model can also be written in terms of Cauchy stress and principle stretches by expressing the principle invariants in terms of *stretch ratio* (Λ), which is the ratio of the undeformed length to the deformed length.

$$\Lambda = 1 - \varepsilon \begin{cases} \Lambda < 1 \Rightarrow \text{compression} \\ \Lambda = 1 \Rightarrow \text{unstretched} \\ \Lambda > 1 \Rightarrow \text{extension} \end{cases} \qquad \textbf{(2.45)}$$

For the uniaxial extension of an incompressible material, stretch ratios for the 3 directions are calculated as below:

$$\left.\begin{array}{l}\Lambda_1 = \Lambda, \\ \Lambda_2 = \Lambda_3, \\ \Lambda_1\Lambda_2\Lambda_3 = 1\end{array}\right\} \begin{array}{l}\Lambda\Lambda_2^2 = 1 \\ \Lambda_2^2 = \Lambda_3^2 = 1/\Lambda\end{array} \quad \textbf{(2.46)}$$

$$\begin{aligned} I_1 &= \Lambda_1^2 + \Lambda_2^2 + \Lambda_3^2 = \Lambda^2 + \frac{2}{\Lambda} \\ I_2 &= \Lambda_1^2\Lambda_2^2 + \Lambda_1^2\Lambda_3^2 + \Lambda_2^2\Lambda_3^2 = 2\Lambda + \frac{1}{\Lambda^2} \end{aligned} \quad \textbf{(2.47)}$$

Substituting these invariants in Equation 2.44, the following equation is obtained:

$$W = C_{10}(\Lambda^2 + \frac{2}{\Lambda} - 3) + C_{01}(2\Lambda + \frac{1}{\Lambda^2} - 3) \quad \textbf{(2.48)}$$

For the simple tension, $\sigma_{11} \neq 0$ and $\sigma_{22} = \sigma_{33} = 0$.

$$\sigma_{11} = \Lambda_1 \frac{\partial W}{\partial \Lambda_1}, \quad \sigma_{33} = \Lambda_2 \frac{\partial W}{\partial \Lambda_2} \quad \textbf{(2.49)}$$

$$\sigma_{11} - \sigma_{33} = 2C_{10}(\Lambda^2 - \frac{1}{\Lambda}) - 2C_{01}(\frac{1}{\Lambda^2} - \Lambda) \quad \textbf{(2.50)}$$

Since $\sigma_{33} = 0$, the Cauchy stress is obtained as the following equation:

$$\sigma_{11} = \left(2C_{10} + \frac{2C_{01}}{\Lambda}\right)\left(\Lambda^2 - \frac{1}{\Lambda}\right) \quad \textbf{(2.51)}$$

As the experimental data contians the true stress and stretch values, the material coefficients for the Mooney-Rivlin material model can also be found by fitting the data to the equation obtained in Equation 2.51. This equation is used to determine the coefficients in this study and the coefficients found by this way will be given in the results section.

2.3.2.2 Yeoh Material Model

The Yeoh hyperelastic model is a model for the deformation of almost incompressible nonlinear elastic materials.

The elastic properties of the material is described using a strain energy density function that is a power series function of the strain invariant only I_1. Yeoh model is also named as *reduced polynomial model* because a polynomial form of the strain energy density function is used but all the three invariants of the left Cauchy-Green deformation tensor are not used.

The strain energy density function of the Yeoh model is as follows:

$$W = C_{10}(I_1 - 3) + C_{20}(I_1 - 3)^2 + C_{30}(I_1 - 3)^3 \qquad \textbf{(2.52)}$$

The true stress equation for this material model can be obtained too, from its energy density function, by a similar way it is done for the Mooney-Rivlin model in the previous section.

With the assumption of $\sigma_{22} = \sigma_{33} = 0$ for the simple tension of an incompressible in one direction, the true stresses are calculated as in the following equations:

$$\sigma_{22} = \sigma_{33} = -p + \frac{2}{\Lambda}\frac{\partial W}{\partial I_1} = 0 \quad \Rightarrow \quad p = \frac{2}{\Lambda}\frac{\partial W}{\partial I_1} \qquad \textbf{(2.53)}$$

$$\sigma_{11} = -p + 2\Lambda^2 \frac{\partial W}{\partial I_1} \qquad \Rightarrow \quad \sigma_{11} = -\frac{2}{\Lambda}\frac{\partial W}{\partial I_1} + 2\Lambda^2 \frac{\partial W}{\partial I_1} \qquad \textbf{(2.54)}$$

$$\frac{\partial W}{\partial I_1} = C_{10} + 2C_{20}(\Lambda^2 + \frac{2}{\Lambda} - 3) + 3C_{30}(\Lambda^2 + \frac{2}{\Lambda} - 3)^2 \qquad \textbf{(2.55)}$$

Substituting Equation 2.55 in Equation 2.54 gives the true stress equation of the Yeoh material model (Equation 2.56).

$$\sigma_{11} = \left(\Lambda^2 - \frac{1}{\Lambda}\right)\left[2C_{10} + 4C_{20}\left(\Lambda^2 + \frac{2}{\Lambda} - 3\right) + 6C_{30}\left(\Lambda^2 + \frac{2}{\Lambda} - 3\right)^2\right] \qquad \textbf{(2.56)}$$

This equation is also used to determine the coefficients in this study and the coefficients found by this way will be given in the results section.

2.3.3 Viscoelasticity Models

2.3.3.1 Linear Viscoelasticity

Linear viscoelasticity is expressed in terms of the Boltzmann integral,

$$\sigma(t) = \int_0^t g(t-\tau)\frac{d\varepsilon(\tau)}{d\tau}d\tau \qquad \textbf{(2.57)}$$

where $g(t)$ is the relaxation function, $\sigma(t)$ is stress, $\varepsilon(t)$ is strain, depending on time t and τ is the integtaion variable in terms of time [11]. The form of the relaxation function and how it is constructed are explained in Section 2.2.2.

2.3.3.2 Nonlinear Viscoelasticity

Nonlinear viscoelasticity models feature the dependence of relaxation function on the strain level as can be seen in the following equation:

$$\sigma(t,\varepsilon) = \int_0^t g(t-\tau,\varepsilon(\tau))\frac{d\varepsilon(\tau)}{d\tau}d\tau \qquad \textbf{(2.58)}$$

2.3.3.3 Quasilinear Viscoelasticity

Fung [9] proposed the quasilinear viscolasticity which is again dependent on both time and strain as in nonlinear viscoelasticity, but it is formulated as the product of two seperate functions: a function of time and a function of strain.

$$g(t,\varepsilon) = g_r(t)h(\varepsilon) \qquad \textbf{(2.59)}$$

$$\sigma(t,\varepsilon) = \int_0^t g_r(t-\tau)\frac{d\sigma}{d\varepsilon}\frac{d\varepsilon(\tau)}{d\tau}d\tau \qquad \textbf{(2.60)}$$

It is obvious that stress depends on strian, however time dependence of stress is independent of strain. Therefore, this formulation is called *quasilinear*. This approach has been seen to fit the experimental data showing the relaxation response of soft tissues quite well [11].

3. UNIAXIAL COMPRESSION EXPERIMENTS

3.1 Mechanical Testing of Soft Tissues

Constitutive eqution presented in the previous section are to abstract the natural behavior of soft, more specifically bovine liver. Even though fluid and solid mechanics mostly base on these definitions and equations, soft biological tissues behave more complicatedly when compared to the industrial (artificial or synthetic) materials. Therefore, simplifications made to construct the constitutive equations need to be compensated by an accurate determination of the coefficients in the equations. These coefficients, which are also called material coefficients, material parameters or material constants, are obtained by a series of material tests.

The methods of testing the mechanical properties of biological tissues do not significantly differ from testing the industrial materials. Material tests for both types of materials can be classified as compression tests, tension tests or cycling tests and these tests also can be conducted uniaxially or biaxially. Uniaxial tests are applied on one single axis where biaxial tests have two perpendicular directions; decision should be made according to the material structure whether it is isotropic, anisotropic or orthotropic. Compression and tension tests basically make difference by the sign of the strain. But some aspects of soft tissues which make them more complicated to model, should be taken into account for the experimental setup. These aspects are mainly the heterogenity of soft tissues and deterioration of soft tissues in vitro conditions. Therefore, the evaluation of results of the experiments and the computations based on them need to be done by considering the type of the tested material, the method of testing, calibration of the testing device and other testing environments that may effect the test data.

Up to now, as also mentioned in the literature review section, so many experiments are performed on different soft tissues in different conditions and by different methods and devices, all trying to have the best results in their own conditions by paying attention to the

above mentioned matters. For example, Carter (2001) carried out his indentation experiments uniaxially in vivo during an open surgery operation on human liver by using a hand-held probe [1]. Kerdok (2006) aimed to obtain more realistic material parameters for in-vitro swine liver by building such an experimental setup that the blood circulation was simulated by a perfusion mechanism [3].

3.2 Experimental Setup and the Testing Device

3.2.1 The LFPlus Material Testing Machine

The following figure is of the device that all the experiments are performed by.

Figure 3.1 : Material testing machine.

It is the single column bench mounted LFPlus materials testing machine of Lloyd Instruments™. Its force capacity is 1kN, speed range is between 0.05 and 1270 mm/min (with maximum 0.2% accuracy at steady state), minimum load resolution is 0.00001 N (with <0.5% load cell accuracy), extension resolution is smaller than 2 microns, data sampling rate is 8 kHz and load measuring system is EN ISO 7500:2004 Class 0.5 ASTM E4.

Its operating temperature range is 5˚ to 35˚C. Test data is collected by a software named NEXYGENPlus to the computer connected to the testing machine.

3.2.2 Materials: Aquaflex Ultrasound Gel Pad & Bovine Liver

The experiments are conducted on two different materials. One is an artificial medical material, Aquaflex® Ultrasound Gel Pad, which is originally used in therapeutic ultrasound procedures. The second material is bovine liver. Aquaflex® Ultrasound Gel Pad is a plate-shaped circular pad with a 90 mm diameter and 20 mm height. It is not viscous as can be seen in Figure 3.2 even though it is named as a gel. Its density is 1.03 g/cc and it can be stored safely between 5˚C and 57˚C. The reason that this gel material is chosen to detect its material properties is that it is foreseen to have a viscoelastic behavior. The tests are performed, first to see whether it shows nonlinear and viscoelastic deformation and second to determine the material constants using the experimental data if the first aim is achieved. The main goal to determine the characteristics of this material is to be able use it as a control material beside real soft tissues. Material tests on biological tissues, face with very important problems such as unclear boundary conditions, heterogeneous structure of the material or the ambiguousness of the applied force which lead to unrepeatability of the experiments in desired conditions. On the other hand, in virtual surgery simulations, doing simplifications on the model and/or some assumptions on the solution process, for they are expected to work real-time, cause the model to diverge from reality. In this case, it becomes difficult to compare the model results to the real behavior. Because the experiments cannot be carried out in all conditions that can be simulated by the mathematical models, even though the models are constructed by the soft tissue's constants, the results of the simulations and the accuracy of the constitutive equations cannot be validated with the limited number of experiments conducted on that soft tissue. Unlimited number of experiments in numerous different conditions can be conducted on an artificial easy-to-find material by benefiting from its well-defined geometric dimensions and boundary conditions. This provides us to obtain data for the desired deformations but certainly if the coefficients of the material is close to the subject soft tissue's coefficients in an allowable degree.

In this study, this artificial material is exposed to indentation experiments to detect its similarity with liver.

Figure 3.2 : Experimental setup with Aquaflex® Ultrasound Gel Pad.

Figure 3.3 : Experimental setup with Aquaflex® Ultrasound Gel Pad.

3.3 Experiments

Two types of experiments are performed on both materials: static indentation tests and ramp-hold tests. Steel probes with 2, 4, 6 and 8 mm radii are attached to the testing machine in order to do the pressing to the material.

For the artificial material (Aquaflex® Ultrasound Gel Pad), water, which is the component that gives its viscous property, is conserved by covering the material with a thin stretch film.

Experiments are conducted in-vitro.

3.3.1 Static Indentation Tests

Static indentation tests are the tests that the material is pressed to a defined depth with a defined constant speed.

Aquaflex® Ultrasound Gel Pad tests are done at two different speeds 0.1 mm/s and 0.5 mm/s by the probes with the radii of 2, 4 and 6 mm where deformation depth is chosen as 2, 4, 6, 8 and 10 mm. Tests are repeated twice and each of them are conducted on a different location on the gel in a limited centeral area in order to eliminate the misleading effects of deformation history. The data obtained from these tests are graphed as below (Figures 3.4, 3.5, and 3.6).

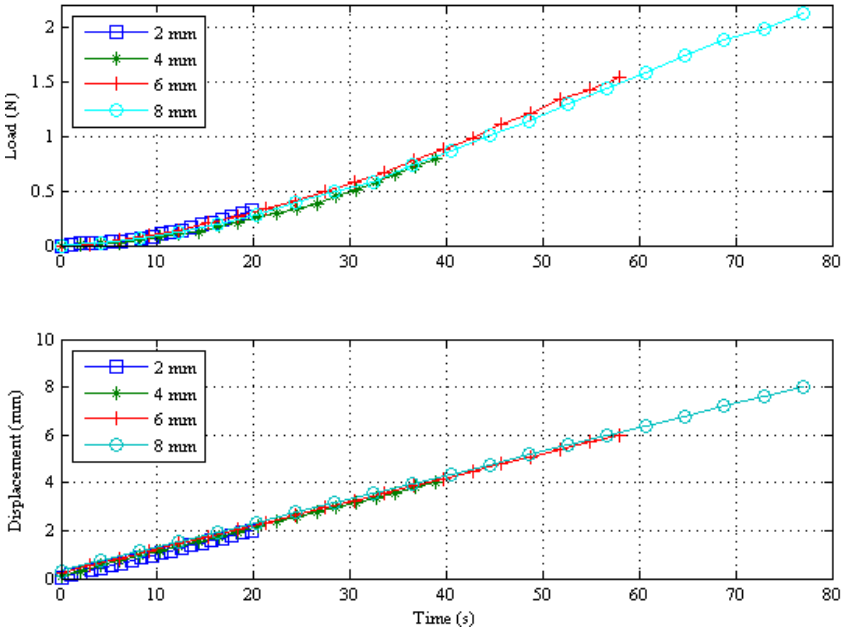

Figure 3.4 : The load-time and displacement-time curves of the indentations of 2, 4, 6 and 8 mm depths with the probe of 2mm radius and strain rate of 0.1 mm/s.

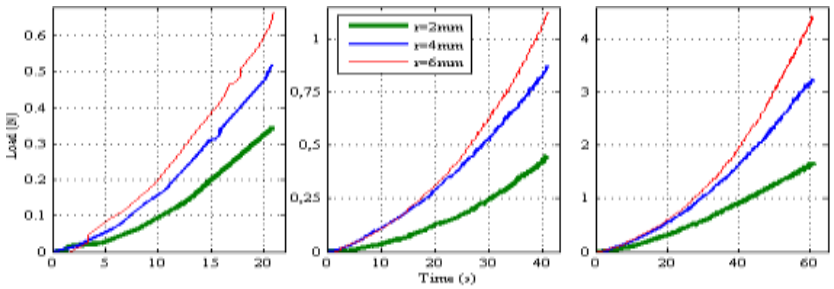

Figure 3.5 : The load-time curves of the indentation tests with threee different probes (2, 4 and 6 mm radii) at 2, 4 and 6 mm depths respectively and with the strain rate of 0.1 mm/s.

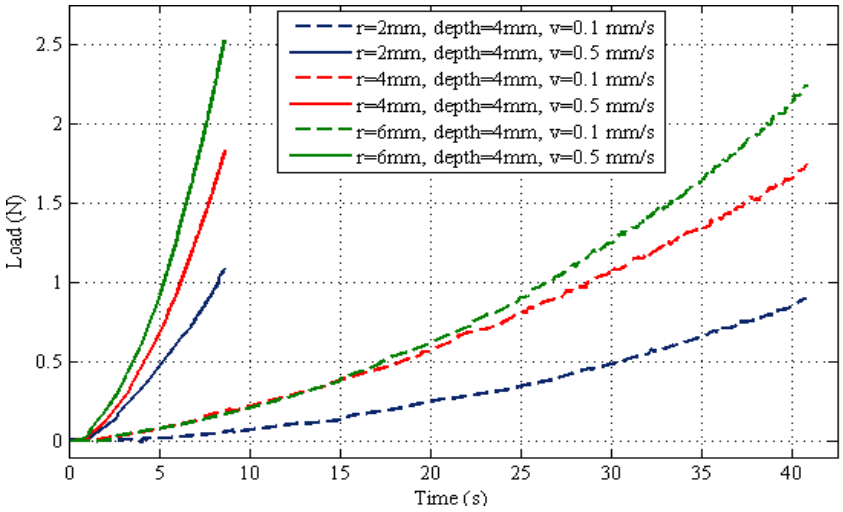

Figure 3.6 : The load differences for the same indentation depth but different strain rates, 0.1 and 0.5 mm/s.

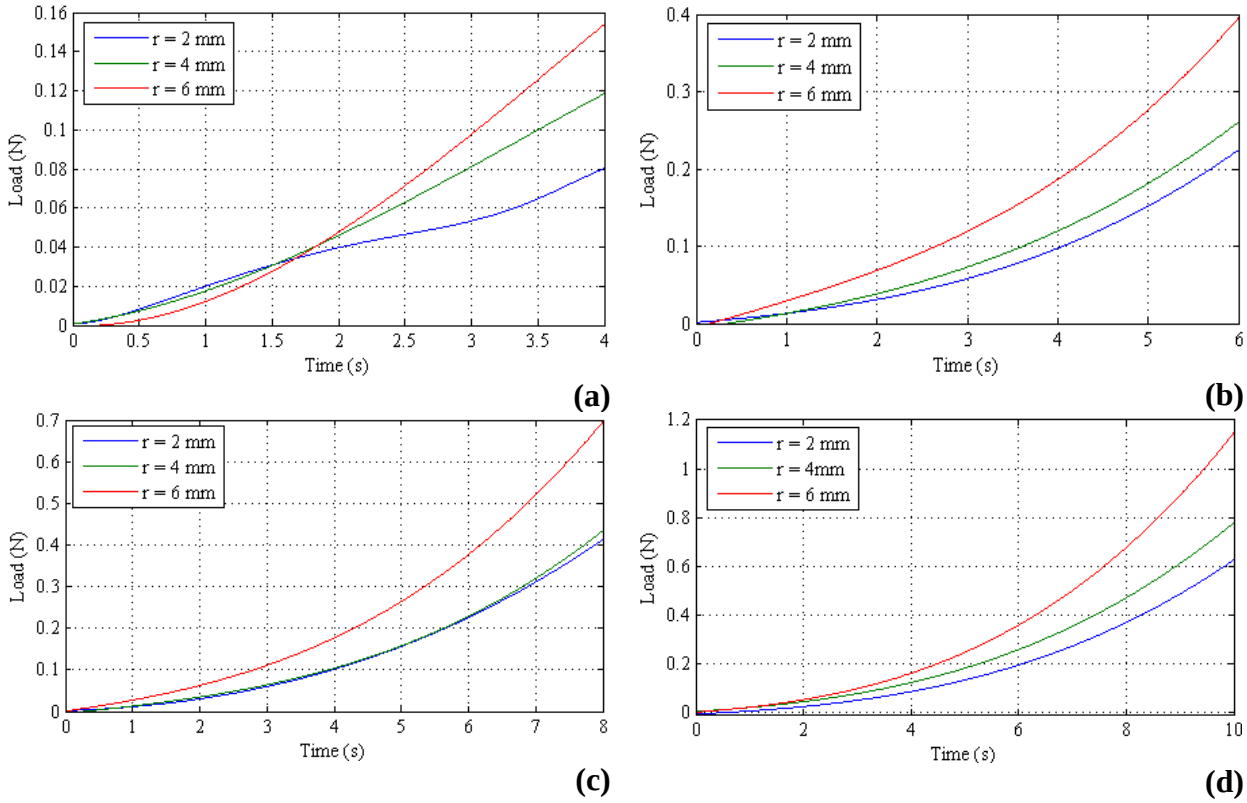

Figure 3.7 : Load-time curves of liver constructed from the static indentation tests with probes of r = 2, 4 and 6 mm at (a) 4 mm, (b) 6 mm, (c) 8 mm and (d) 10 mm depths.

Bovine liver was also exposed to in-vitro static indentation tests. The livers were stored in the serum solution right after removing it from the animal and before using for material testing. Two livers were exposed to material testing; one was used as a whole for the standart static

indentation and ramp-hold tests, the other one was used for axial tests in order to determine whether or not its material properties depend on the application axis.

The static indentation tests conducted on the complete liver were done with the 2, 4 and 6 mm-radius probes to the depths of 4, 6, 8 and 10 mm, repeating each test twice and measuring the thickness of each indentation point. Results are shown in the Figures 3.7 and 3.8.

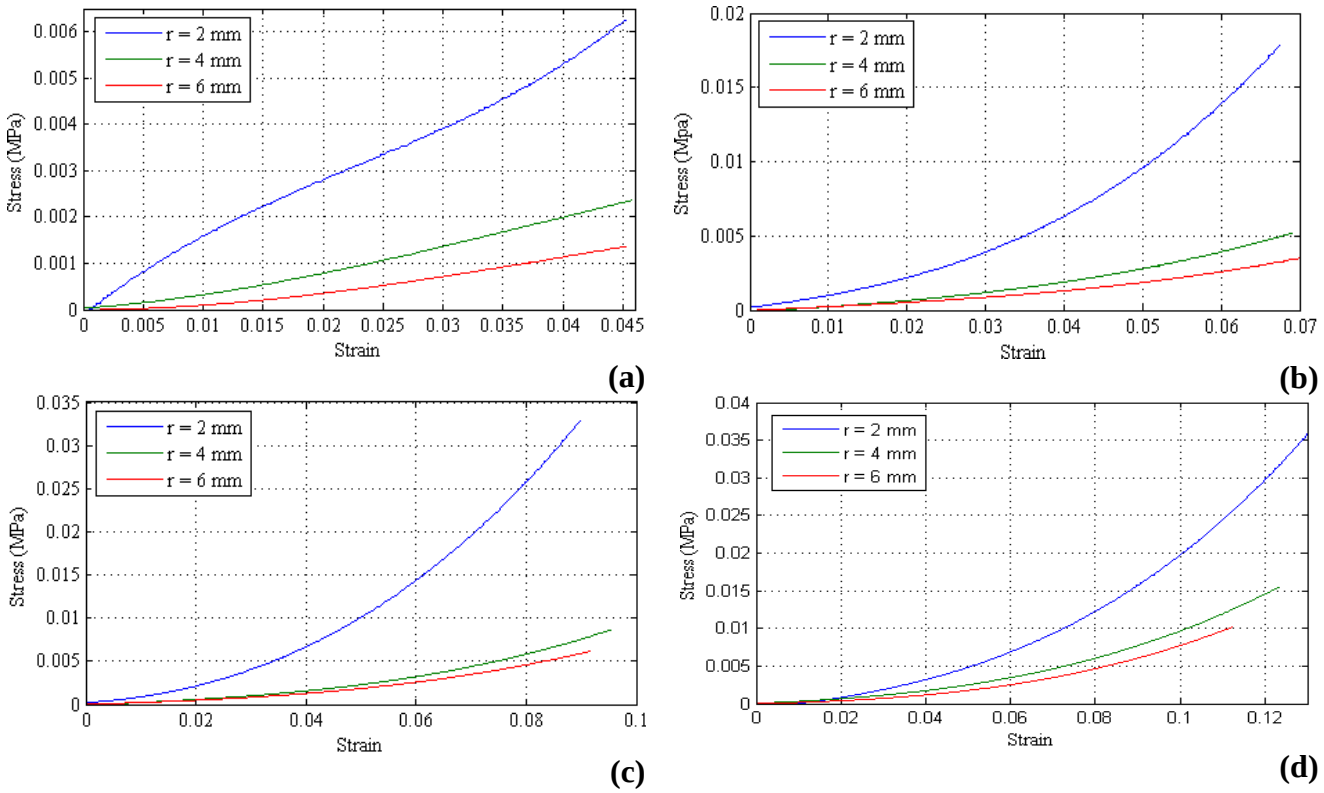

Figure 3.8 : Stress-strain curves constructed from the static indentation tests conducted on liver with the probes of r=2, 4 and 6 mm at (a) 4 mm, (b) 6 mm, (c) 8 mm and (d) 10 mm depths.

3.3.1.1 Axial Material Tests on Bovine Liver

In order to obtain the anisotropic behavior of the liver, there is a need to conduct the axial tests. Axial tests were static indentation tests conducted on the cube-like liver parts cut out from the bovine liver. It is important to note that each axis of the cubic-like part are marked and tests are conducted on each face of the cubic geometry based on three different axes. First, one cube-like part was tested on its three different axes. Secondly three cube-like liver parts are excised and tests are conducted on each part on a different direction. The membrane on the surface on one part was removed to get rid of its extra effect because the other two parts had no membranes.

First type axial tests, static indentations, were performed on one cube-like liver part with a strain rate of 0.1 mm/s with the 2 mm-radius probe to the depths of 4 and 8 mm. Tests were repeated twice and each test was conducted on a different location provided that the thickness was measured. The measurements are graphed as below (Figure 3.9).

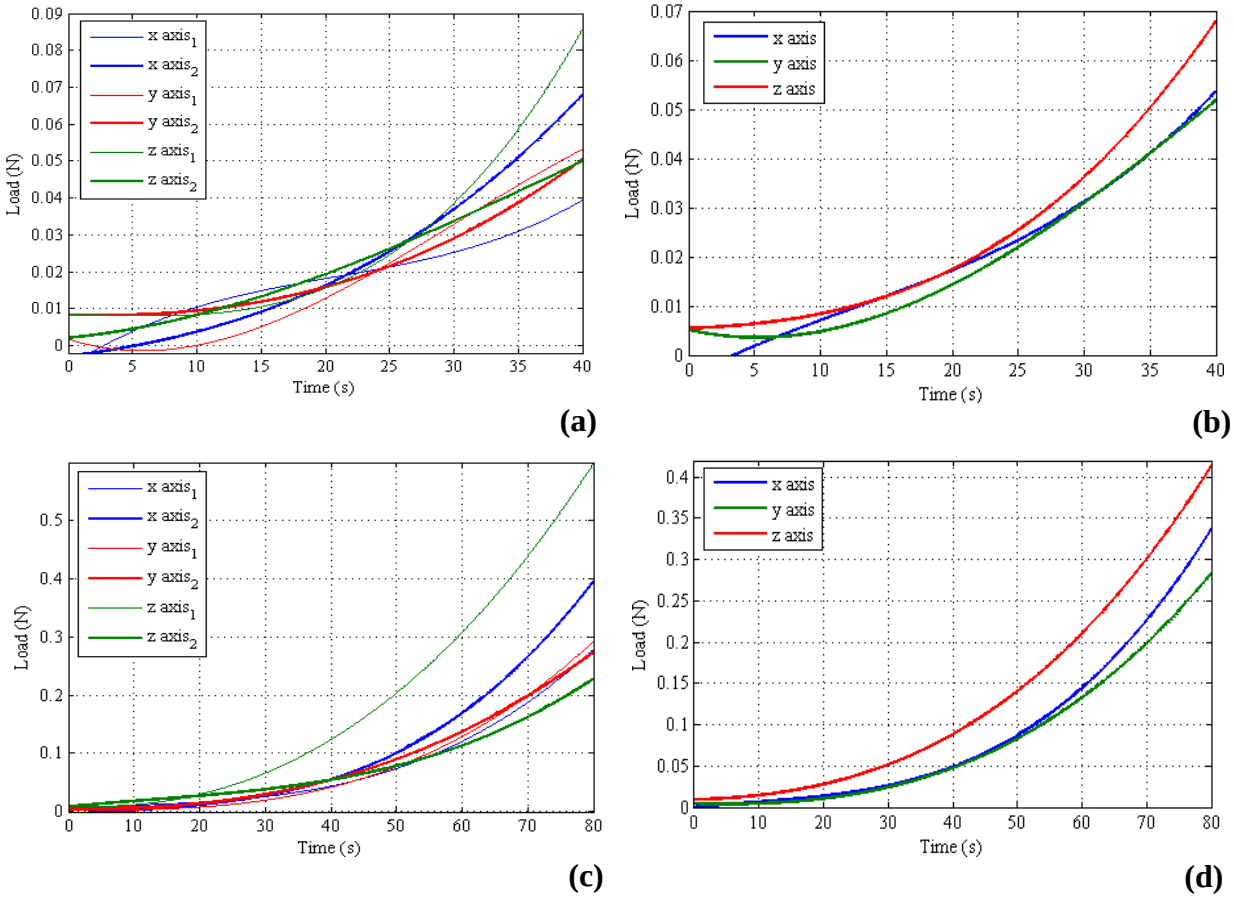

Figure 3.9 : Load-time curves constructed from the axial static indentation tests conducted on liver with the probe of 2 mm radius at (a and b) 4 mm depth and (c and d) 8 mm depth.

The second type axial tests, which were done on 3 different cubes, were static indentations to a depth of 5 mm, which was chosen to be appropriate according to the dimensions of the cubes, with the 2 mm-radius probe. The measurements are visualized as below (Figure 3.10).

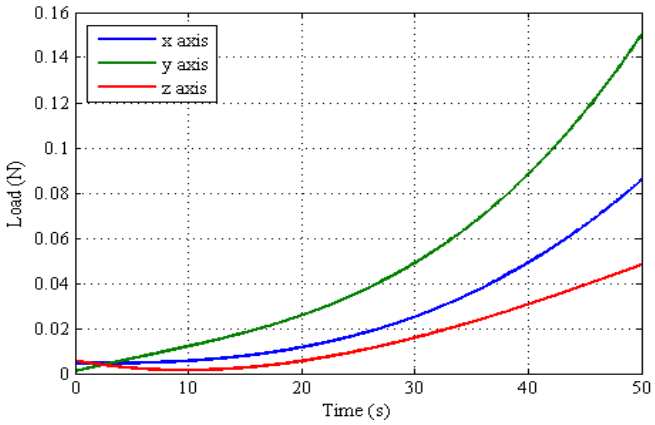

Figure 3.10 : Load-time curves constructed from the axial static indentation tests conducted on three different cube-like liver parts, with the probe of 2 mm radius at 5 mm depth.

3.3.2 Ramp – Hold Tests

Ramp-hold tests are performed to detect the relaxation behavior of materials. The materials are deformed to a defined depth and the deformation is held for a while to record the change in loading which would be a decrease for the case of viscoelasticity.

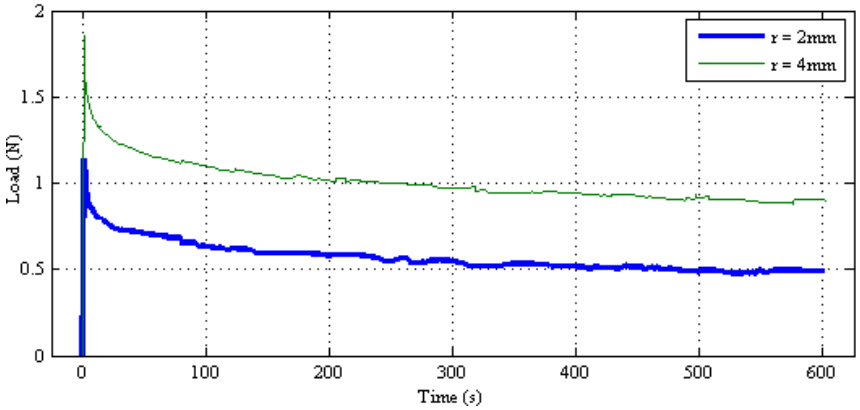

Figure 3.11 : The load-time curves constructed from the 4 mm displacement tests conducted on the gel with probes of 2 and 4 mm radii; indented in 1 s and held for 600 s

Ramp-hold tests are conducted on Aquaflex® Ultrasound Gel Pad in the same experimental conditions. The gel is deformed to depths of 2, 4 and 6 mm with 2, 4 and 6 mm radii-probes and the deformation is kept constant for 600 seconds. Each test is conducted on a different location in a limited central area again as in the static deformation tests. Figure 3.11 and Figure 3.12 present the gel's behavior under deformation obtained as the result of these material tests.

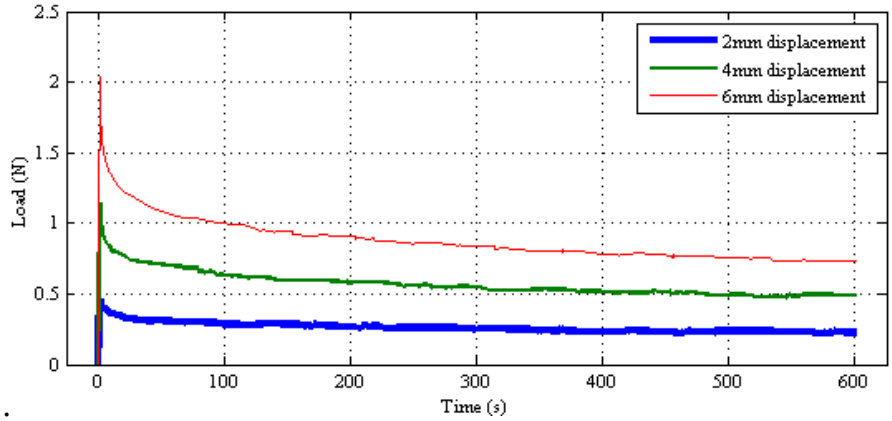

Figure 3.12 : The load-time curves of the relaxation tests at 2,4 and 6 mm depths conducted on the gel with 2mm-radius-probe; indented in 1 s and held for 600 s.

In-vitro relaxation tests on the bovine liver were performed on a whole liver. The same experimental setup and tools are used for the experiments.

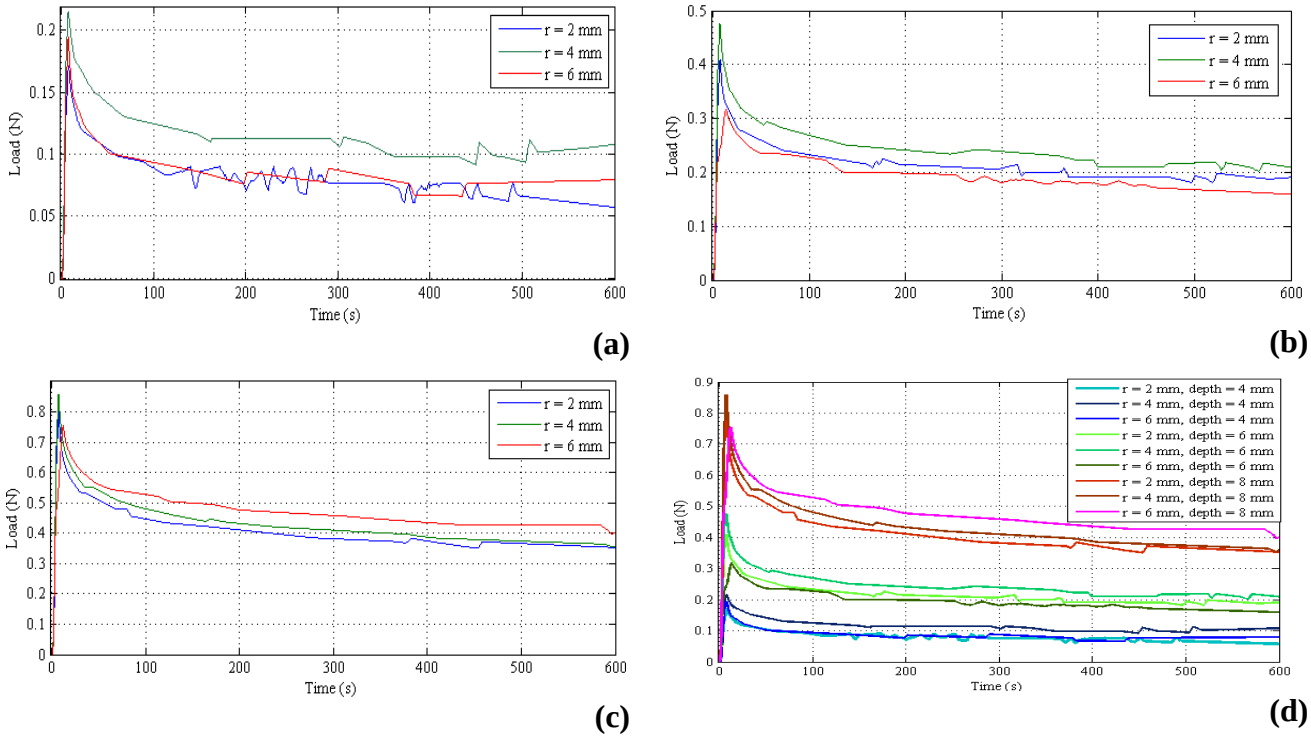

Figure 3.13 : Load-time curves constructed from the ramp-hold tests conducted on liver with the probes of 2, 4, and 6 mm radii at (a) 4 mm depth, (b) 6 mm depth, (c) 8 mm depth. (d) shows the curves at all depths with the three different probes.

Probes with radii of 2, 4 and 6 mm are used. Indentation depth was chosen to be 4, 6 and 8 mm where each indentation was performed with a certain strain rate so that the indentation was completed in 1 second. Tests were repeted twice on different points for precision and

thickness values were taken for strain measurement. Test data is graphed in Figure 3.13 and figure 3.14.

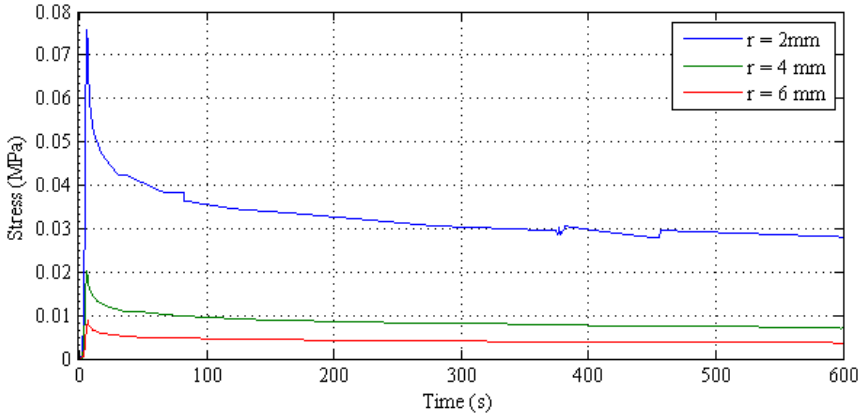

(a)

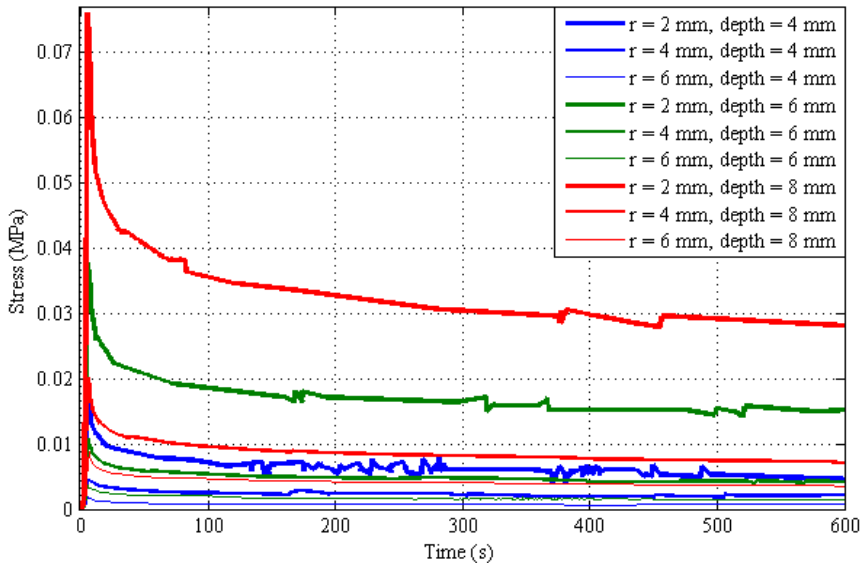

(b)

Figure 3.14 : Stress-strain curves constructed from the ramp-hold tests conducted on liver with the probes of 2, 4, and 6 mm radii at (a) 8 mm depth, and at (b) 4, 6, and 8 mm depths.

4. FINITE ELEMENT MODELING

This thesis aims to find the material coefficients via inverse Finite Element Method (inverse FEM). Inverse FEM, which necessitates to construct the FE models of the experiments, is explained in details in the next section; here in this section the construction of the testing models are explained. For the FE models of this study, the commercial finite element software Abaqus (Version 6.7) is used.

4.1 Finite Element Analysis

Finite Element Analysis (FEA) is a numerical method to solve engineering problems that seek, for example, the stress distribution, the temperature change or the displacements of each point on a part. When the geometry, the boundary and loading conditions of the problem get more complex, it becomes harder, even impossible, to solve the problem analytically, therefore, it becomes necessary to use this finite element or a similar numerical approach.

The finite element method is first developed to calculate the stress distributions on the aircrafts [22], however now it is used for various fields of continuum mechanics such as biomechanics.

In finite element analysis, a virtual model of the real structure is created; the structure is modeled as the combination of small pieces which are called *finite elements*. The term finite is used to prevent confliction with the infinitesimal elements of the calculus. These finite elements connect to each other at points which are called *nodes*. The combination of some elements makes the finite element structure and a particular arrangement of the elements is called a *mesh* [22]. The finite element mesh of a structure is shown in Figure 4.1.

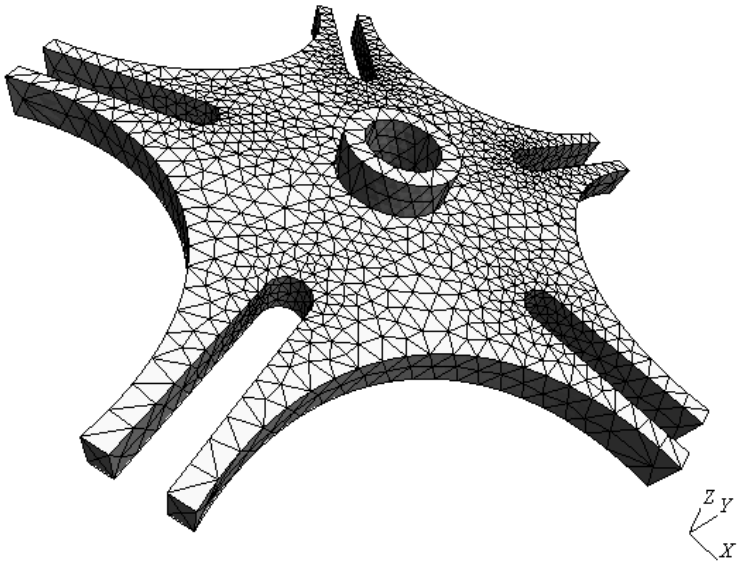

Figure 4.1 : The finite element mesh of a structure [27].

In the FEA, the values of the field variables on the elements are approximated by polynomial functions that can simulate the real, more complicated variations of those variables. And the governing differential equations or integral expressions are transformed into a set of linear algebraic equations [22].

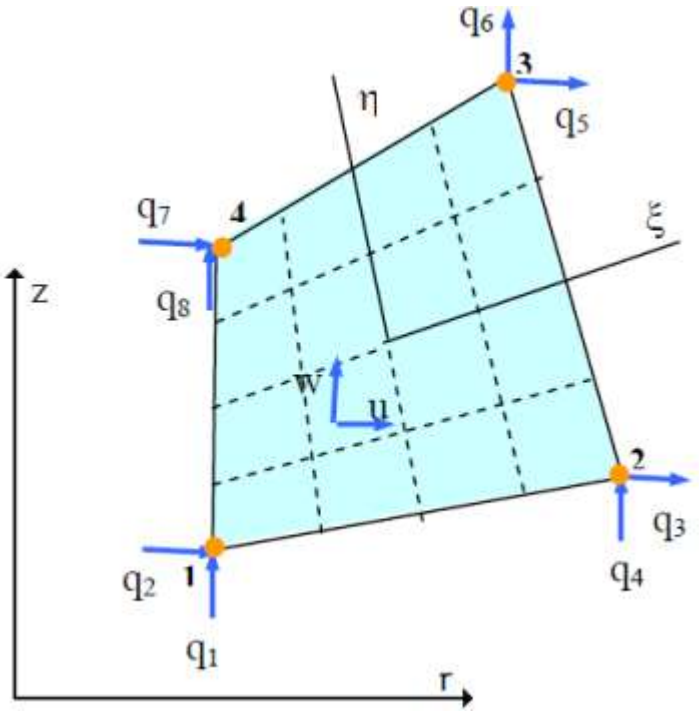

Figure 4.2 : An axisymmetric quadrilateral linear element [22].

The FEA formulation can be constructed by using etiher a differential equation formulation method or a variational formulation method. Displacement method,

force method and displacement-force method are the differential equation formulation methods; principle of minimum potential energy, principle of minimum complementary energy and principle of stationary Reissner energy are the variational formulation methods. Below is the summary of the basic FE formulation [22].

In a finite element analysis, a number of basic equations must be satisfied: equations of strain displacement relations, governing equations, equilibrium equations compatibility equations and boundary conditions. Let's consider the formulation for an axisymmetric quadrilateral linear element (Figure 4.2).

The generic displacements for any point on the axisymmetric element are:

$$\{\delta\} = \begin{bmatrix} u & w \end{bmatrix}^T \tag{4.1}$$

The nodal displacement vector is:

$$\{\delta\} = [u_1 \quad w_1 \quad \dots \quad u_4 \quad w_4]^T = [q_1 \quad q_2 \quad \dots \quad q_8]^T \tag{4.2}$$

Using the interpolation functions (shape functions) N_1, N_2, N_3 and N_4, displacements can be expressed with the following displacement functions:

$$\begin{aligned} u &= N_1 u_1 + N_2 u_2 + N_3 u_3 + N_4 u_4 \\ w &= N_1 w_1 + N_2 w_2 + N_3 w_3 + N_4 w_4 \end{aligned} \tag{4.3}$$

in which the shape functions, in terms of dimensionless coordinates, are as follows:

$$\begin{aligned} N_1 &= (1/4)(1-\xi)(1-\eta) \\ N_2 &= (1/4)(1+\xi)(1-\eta) \\ N_3 &= (1/4)(1+\xi)(1+\eta) \\ N_4 &= (1/4)(1-\xi)(1+\eta) \end{aligned} \tag{4.4}$$

In the matrix form:

$$\{\delta\} = \begin{Bmatrix} u \\ w \end{Bmatrix} = \begin{bmatrix} N_1 & 0 & N_2 & 0 & N_3 & 0 & N_4 & 0 \\ 0 & N_1 & 0 & N_2 & 0 & N_3 & 0 & N_4 \end{bmatrix} \begin{Bmatrix} q_1 \\ q_2 \\ \vdots \\ q_8 \end{Bmatrix} \tag{4.5}$$

Concisely:

$$\{\boldsymbol{\delta}\}_i = [\boldsymbol{N}]_i \{\boldsymbol{q}\}_i \qquad (i = 1,2,3,4) \tag{4.6}$$

u_i and w_i are the translations in the r and z directions, respectively. For this is an axisymmetric element that forms the solid by revolution, the translation v in the θ direction is zero; the shearing strains $\gamma_{r\theta}$ and $\gamma_{z\theta}$ are zero.

The non-zero strain components are as follows:

$$\{\boldsymbol{\varepsilon}\}_i = [\varepsilon_r \quad \varepsilon_z \quad \varepsilon_\theta \quad \gamma_{rz}]_i^T \tag{4.7}$$

The strain-displacement relation is as follows:

$$\begin{Bmatrix} \varepsilon_r \\ \varepsilon_z \\ \varepsilon_\theta \\ \gamma_{rz} \end{Bmatrix}_i = \begin{bmatrix} \frac{\partial}{\partial r} & 0 \\ 0 & \frac{\partial}{\partial z} \\ \frac{1}{r} & 0 \\ \frac{\partial}{\partial z} & \frac{\partial}{\partial r} \end{bmatrix} \begin{Bmatrix} u \\ w \end{Bmatrix}_i \tag{4.8}$$

$$\{\boldsymbol{\varepsilon}\}_i = [\partial]\{\boldsymbol{\delta}\}_i = [\partial][\boldsymbol{N}]_i \{\boldsymbol{q}\}_i = [\boldsymbol{B}]_i \{\boldsymbol{q}\}_i \tag{4.9}$$

$$\text{where } [\partial] = \begin{bmatrix} \frac{\partial}{\partial r} & 0 \\ 0 & \frac{\partial}{\partial z} \\ \frac{1}{r} & 0 \\ \frac{\partial}{\partial z} & \frac{\partial}{\partial r} \end{bmatrix} \text{ and } [\boldsymbol{B}]_i = [\partial][\boldsymbol{N}]_i . \tag{4.10}$$

The radius r in Equation 4.10 is calculated as:

$$r = \sum_{i=1}^{4} N_i r_i \tag{4.11}$$

The four stress components corresponding to the strain components are:

$$\{\boldsymbol{\sigma}\}_i = [\sigma_r \quad \sigma_z \quad \sigma_\theta \quad \tau_{rz}]_i^T \tag{4.12}$$

The shearing stresses $\tau_{r\theta}$ and $\tau_{\theta z}$ are also zero. Then, the governing relation for a linear elastic material, which is the stress-strain relationship, is given in matrix form as below:

$$\{\boldsymbol{\sigma}\}_i = [\boldsymbol{E}]\{\boldsymbol{\varepsilon}\}_i \tag{4.13}$$

Here, $[\boldsymbol{E}]$ is the matrix of elasticity constants (Young's modulus), that is already explained in the second section.

$$\begin{Bmatrix} \sigma_r \\ \sigma_z \\ \sigma_\theta \\ \gamma_{rz} \end{Bmatrix}_i = \begin{bmatrix} E_{11} & E_{12} & E_{13} & E_{14} \\ & E_{22} & E_{23} & E_{24} \\ & & E_{33} & E_{34} \\ & sym. & & E_{44} \end{bmatrix} \begin{Bmatrix} \varepsilon_r \\ \varepsilon_z \\ \varepsilon_\theta \\ \tau_{rz} \end{Bmatrix}_i \tag{4.14}$$

The strain energy of a linear elastic body is defined as

$$U = \frac{1}{2}\int_V \{\boldsymbol{\varepsilon}\}^T [\boldsymbol{E}]\{\boldsymbol{\varepsilon}\} dV \tag{4.15}$$

On the other hand, the total potential energy of the element can be expressed with the stiffness matrix $[k]$ as follows:

$$\frac{1}{2}\int_V \{\boldsymbol{q}\}^T [\boldsymbol{k}]\{\boldsymbol{q}\} dV \tag{4.16}$$

From Equation 4.15 and 4.16, it can be derived that $[\boldsymbol{k}] = \int_V [\boldsymbol{B}]^T [\boldsymbol{E}][\boldsymbol{B}] dV$, by substituting Equation 4.9 into Equation 4.15.

As the stiffness matrix is obtained, the basic equation, Hooke's law of elasticity, is ready to be solved in order to find the displacements:

$$F = kx \tag{4.17}$$

For our problem, the nodel displacement vector $\{\boldsymbol{q}\}$ is calculated by the following equation:

$$\begin{Bmatrix} f_1 \\ f_2 \\ \vdots \\ f_8 \end{Bmatrix} = [\boldsymbol{k}] \begin{Bmatrix} q_1 \\ q_2 \\ \vdots \\ q_8 \end{Bmatrix} \qquad \textbf{(4.18)}$$

The solution process for an axisymmetric quadrilateral linear element can be summarized with the previous computational steps. However, the size of the vectors and matrices, the shape of the functions change according the element type while the main procedure do not change. The number of nodes and the degree of the shape function may be increased for a different element type as well as the dimension of the element alters the number of variables.

For the element used in our model, the compatibility conditions, that is, the nodal number of equations and unknowns are as follows:

Displacements: u, w → Equilibrium equations = 2

Strains: $\varepsilon_r, \varepsilon_z, \varepsilon_\theta, \gamma_{rz}$ → Strain-displacement relations = 4

Stresses: $\sigma_r, \sigma_z, \sigma_\theta, \tau_{rz}$ → Constitutive relations = 4

Total equations = 10 → Total unknowns = 10

4.2 The FE Model of the Experiments and the Contact Model

One model is created to simulate the static indentation tests with a hyperelastic material model. Another model is created to simulate the same tests with a viscoelastisity assumption. Two new models are created by modifying them so as to simulate the relaxation tests.

To explain the main structure of the model, an axisymmetric contact model consisting of two different parts, the indentor and the deformed material are used. The indentor is defined as a 2D analytical rigid shell part where the other part is chosen to be a deformable solid which is contructed by a transformation from shell to solid as a requirement of the FE modeling software. To set the contact relation between these two parts, an interaction between each material's contacting surfaces, a rigid body constraint for the indentor and an interaction property that holds the

information about the friction are defined. The interaction property is set to “rough” which means that no slip will occur once the points are in contact.

The contact is based on the finite-sliding formulation where seperation and sliding of finite amplitude and arbitrary rotation of the surfaces may arise. The finite-sliding rigid contact procedure works by a family of contact elements that are automatically generated with respect to the data associated with the defined contact pairs. At each integration point these elements construct a measure of overclosure (the penetration of the point on the surface of the deforming body (master surface) into the rigid surface) and measures of relative shear sliding. These kinematic measures are then used in appropriate Lagrange multiplier techniques to present the appropriate surface contact and friction theories [12].

Finite-sliding formulation allows arbitrary motion of the surfaces. Contact conditions are implemented on the surface of the slave (surface on the indentor) not at discrete points or at slave nodes. This leads to the possibility of observing some penetration at individual nodes; however, large, undetected overclosures do not occur with this discretization [12].

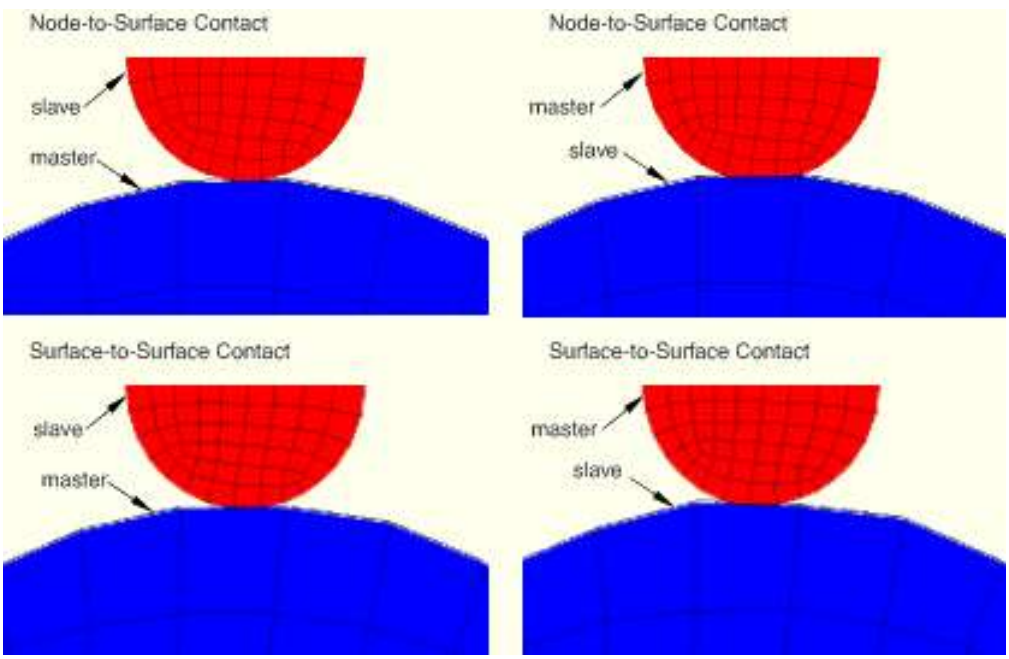

Figure 4.3 : Comparison of contact enforcement for node-to-surface and surface-to-surface contact discretizations [12].

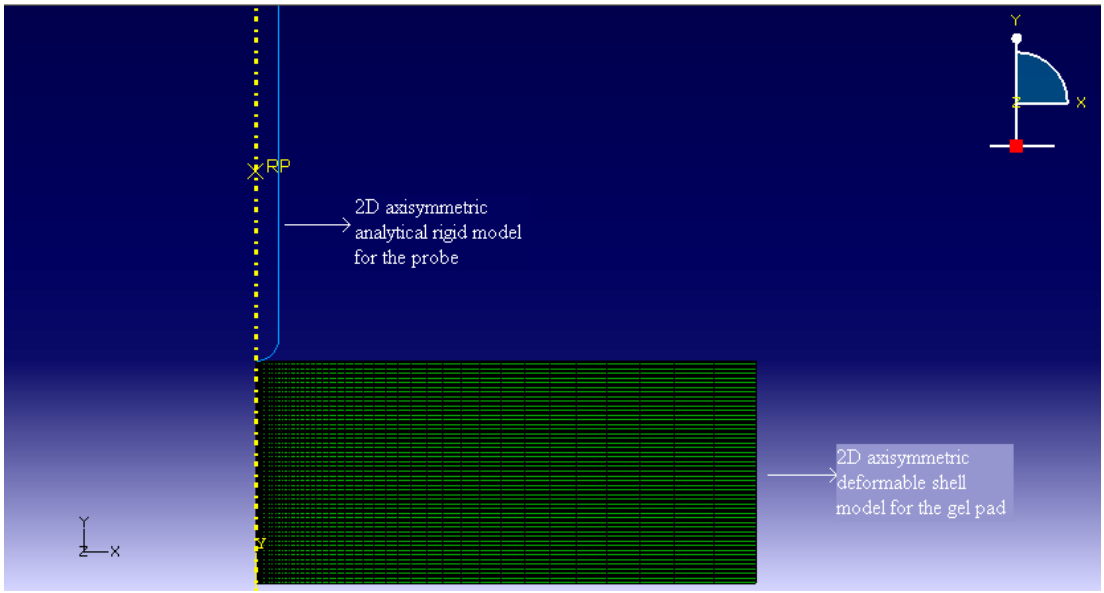

Figure 4.4 : Axisymmetric finite element contact model.

Our FE contact model for undeformed shape is shown in Figure 4.4. The rectangular part is the axisymmetric model of the circular gel pad. To the center of the gel pad, an axisymmetric analytical rigid structure, which is created to simulate the probe, is placed.

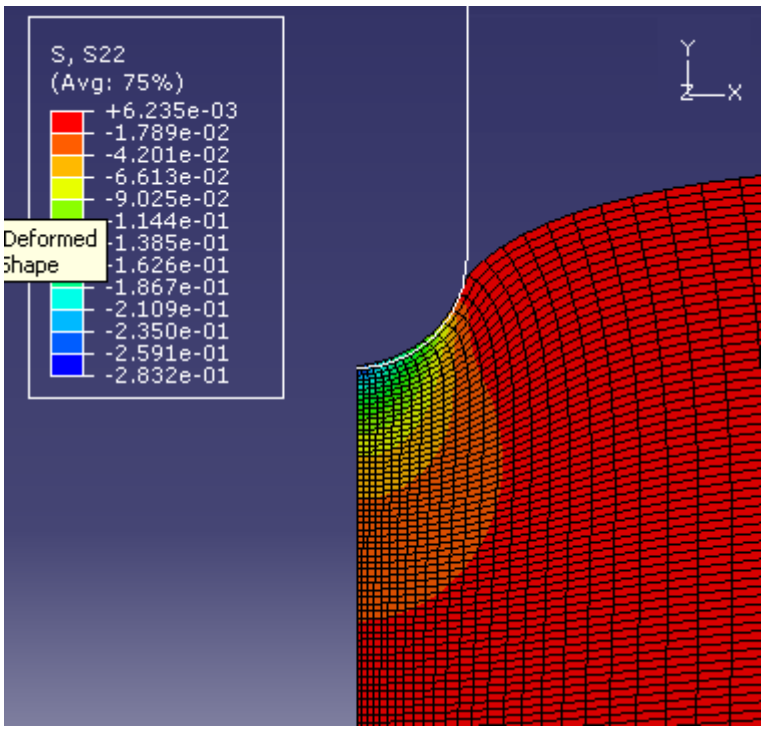

Figure 4.5: The deformed shape of the finite element contact model, showing the stress distribution in the y direction for a ~20% (3.9 mm) deformation (deformation scale factor is 1).

5. INVERSE METHOD

To solve the simulation problem, finite element tools require the material type and material coefficients to be defined in the model. Here, the most important point that requires attention besides constructing the model properly, is to set the accurate material type and coefficients. The closer to the exact values the parameters of the material model are, the more realistic the solution is. There are several numerical methods that can be found in literature to approximate or determine the material coefficients of a material with a specific type. Curve fitting is an option in which the material model stress equations are fitted to the experimental stress data. However, previous studies show that a better approximation can be done by another numerical approach named inverse finite element method.

5.1 Inverse Finite Element Algorithm

Inverse finite element method is an algorithm that runs the model with an initial parameter set and compares the FE result to the experimental data and improves the parameter set with respect to the computed error and pre-defined error tolerance. This procedure continues iteratively until the error between the model and the experiment data is small enough. This algorithm can be built to find any parameter of the model as well as the material coefficients. In details, it is a coupling process of the FE tool with an optimization algorithm; FE tool solves the model using the given parameters, where the optimization tool gets the FE results, makes a better estimation of parameters after computing the error with respect to the test data and sets the new parametrers to the FE model. The flow chart of the algorithm is illustrated as in Figure 5.1. The scripts coded to perform this algorithm is given in Appendix A.1.

5.2 Optimization Methods

Any optimization method can be used in the algorithm as soon as it fits the problem. Some optimization methods are local solvers while some are global. Local solvers stop when a local minimum of the objective function is found, however global

solvers aim to find the minimum of all minima, which is the global minimum of the objective function. However, a global solver doesn't guarantee to find the global minimum; because global methods work so as to reduce the objective function in each optimization step, the method cannot promise to converge for the global minimum, it requires the initial parameters to be very close to real values for a good solution [13].

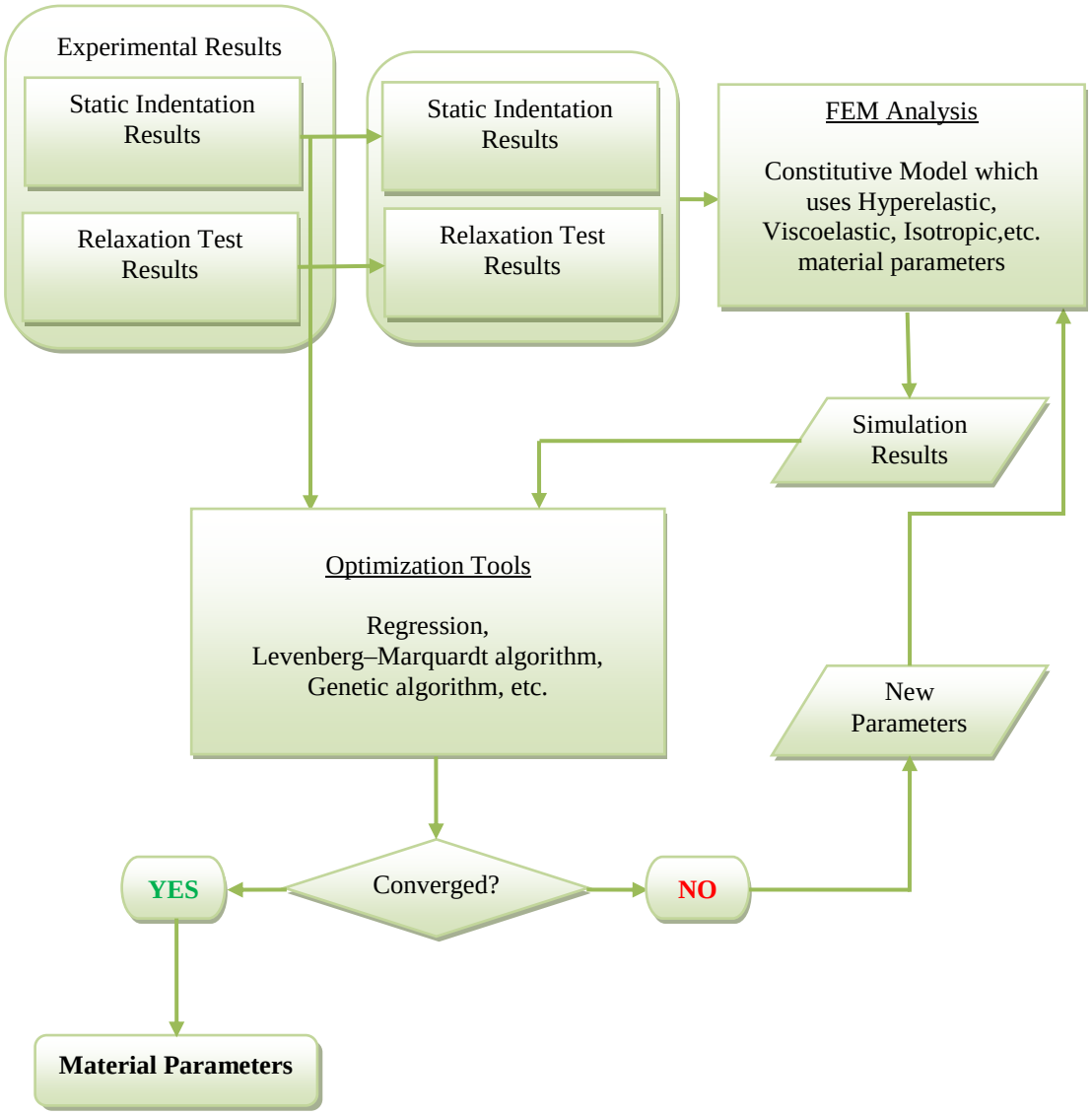

Figure 5.1 : The inverse FE algorithm.

The optimization part of this study is minimizing the residual vector (R_i) which holds the differences between the model data (f_{model}) and experimental data (f_{exp}).

The expression to be minimized is given in equation (5.1) where i is the number of discretized data, t is time and p is the parameter set to be determined.

$$R_i(p) = f_{model}(p, t_i) - f_{exp}(t_i) \quad \textbf{(5.61)}$$

$$\min_p \sum_{i=1}^{n} (R_i(p))^2 \quad \textbf{(5.62)}$$

In this study, some of the optimization methods such as Gauss-Newton, Levenberg-Marquardt, Trust Region and simplex search method are evaluated. Because our objective function is nonlinear, numerical methods for nonlinear optimization are considered.

5.2.1 Theory of the Gauss-Newton Method

For the problem of fitting a function of n parameters to a data vector d, a nonlinear system of equations $G(m) = d$ is tried to be achieved by optimizing the parameters m and minimizing the 2-norm of the residuals [14].

$$f(m) = \sum_{i=1}^{n} (G(m)_i - d_i)^2 \quad \textbf{(5. 3)}$$

If we let

$$f_i(m) = G(m)_i - d_i \qquad i = 1, 2, ..., n \quad \textbf{(5.4)}$$

and

$$\boldsymbol{F}(m) = \begin{bmatrix} f_1(m) \\ \vdots \\ f_n(m) \end{bmatrix} \quad \textbf{(5.5)}$$

we can write

$$f(m) = \sum_{i=1}^{n} f_i(m)^2. \quad \textbf{(5.6)}$$

The gradient of $f(m)$ can be written as

$$\begin{aligned}\nabla f(m) &= \sum_{i=1}^{n} \nabla(f_i(m)^2) \\ &= \sum_{i=1}^{n} 2\nabla f_i(m) f_i(m) \\ &= 2\boldsymbol{J}(m)^T \boldsymbol{F}(m)\end{aligned} \quad \textbf{(5.7)}$$

where $\boldsymbol{J}(m)$ is the Jacobian.

Similarly, the matrix of second derivatives, the Hessian is obtained as follows:

$$\nabla^2 f(m) = 2\boldsymbol{J}(m)^T \boldsymbol{J}(m) + \underbrace{2\nabla(\boldsymbol{J}(m)^T \boldsymbol{F}(m))}_{\boldsymbol{Q}(m)} \quad \textbf{(5.8)}$$

The Gauss-Newton (GM) method omits the $\boldsymbol{Q}(m)$ term [14] thus obtains the Hessian as in equation 5.9.

$$\nabla^2 f(m) \approx 2\boldsymbol{J}^T(m)\boldsymbol{J}(m) \quad \textbf{(5.9)}$$

The GN optimization method converges to a solution when $\nabla f(m) = 0$ is achieved [3]. That is,

$$\boldsymbol{J}^T(m)\boldsymbol{J}(m)\Delta m = -\boldsymbol{J}(m)^T \boldsymbol{F}(m). \quad \textbf{(5.10)}$$

Here, if the $f_i(m)$ terms are reasonably small, then it is a reasonable approximation. But if the terms are large wich means in other words, that $\boldsymbol{J}^T(m)\boldsymbol{J}(m)$ is singular, then the optimization doesn't converge, the Gauss-Newton method fails. The GN method necessitates the term $\boldsymbol{J}^T(m)\boldsymbol{J}(m)\Delta m$ to be positive semi-definite and symmetric [14].

5.2.2 Theory of the Levenberg-Marquardt Method

Levenberg-Marquardt algorithm (LM algorithm) [14] improves the Gauss-Newton method by adding an extra term to the Hessian matrix of the 2nd derivatives of the function in order to eliminate the risk of singularity.

$$\nabla^2 f(m)\Delta m = (\boldsymbol{J}^T(m)\boldsymbol{J}(m) + \lambda \boldsymbol{I})\Delta m, \quad \lambda > 0 \quad \textbf{(5.11)}$$

The positive term $\lambda \boldsymbol{I}$ ensures that the matrix is not singular. It is adjusted at each iteration of the computation so as to provide convergence. Since the matrix in right

hand side of the equation 5.11 is positive-semidefinite and symmetric, the system can be solved via Cholesky factorization [14].

If λ is large, Δm becomes a *steepest-descent* step (Equation 5.13); the method moves down-gradient to reduce $f(m)$, which means a slow yet certain convergence. In contrast, if the additional term is very small, the LM method reverts to the GN method that provides fastness but uncertainity for convergence [14].

$$\boldsymbol{J}^T(m)\boldsymbol{J}(m) + \lambda \boldsymbol{I} \approx \lambda \boldsymbol{I} \quad \textbf{(5.12)}$$

$$\Delta m \approx -\frac{1}{\lambda}\nabla f(m) \quad \textbf{(5.13)}$$

5.2.3 Theory of the Trust Region Methods

Trust region algorithm makes a further improvement by evolving the Levenberg-Marquardt algortihm. In the case of negative curvature, that is, when the Hessian matrix is negative, Gauss-Newton fails and L-M algorithm follows a perturbated and approximate direction of research of Δm based on an arbitrary perturbation of the Hessian. In LM algorithm, choosing a large λ makes the Hessian part of the expression (Equation 5.12) ineffective but, more importantly it has an effect as reducing the step size Δm. Trust Region algorithm focuses on this effect and imposes a proper limitation on the step size as in Equation 5.14 and by this way, succeeds the global convergence even if the approximation of the Hessian matrix is indefinite [15].

$$\Delta n < \Delta_t \text{ (trust region radius)} \quad \textbf{(5.62)}$$

The computation of Δ_t is another constraint minimization of a quadratic expression and this increases the complexity of the Trust Region algorithms (Eq. 5.14) [15].

$$f(m+\Delta n) = \min_{\Delta n}(f(m+\Delta n)) \text{ subject to } \Delta n < \Delta_t \quad \textbf{(5.63)}$$

In Trust Region methods, the Hessian matrix is obtained numerically in several ways, by the well-known BFGS formulae, by the multivariate polynomial interpolation or by the finite difference approximation. Although the multivariate polynomial interpolation is the best to determine the 2nd derivatives, it is a very

time-consuming algorithm [15]. Because Matlab routines is used in this study for optimization, finite difference approximation is preferred in the trust region algorithm as the choice of the Matlab routine.

5.3 Validation of the Inverse Method

Our inverse finite element algorithm is first checked by a simple finite element model that involves a beam element made of steel. Parameters to be found is Young's modulus for the case of known Poisson's ratio. The beam model together with the visualisation of the deformed shape is shown in Figure 5.2.

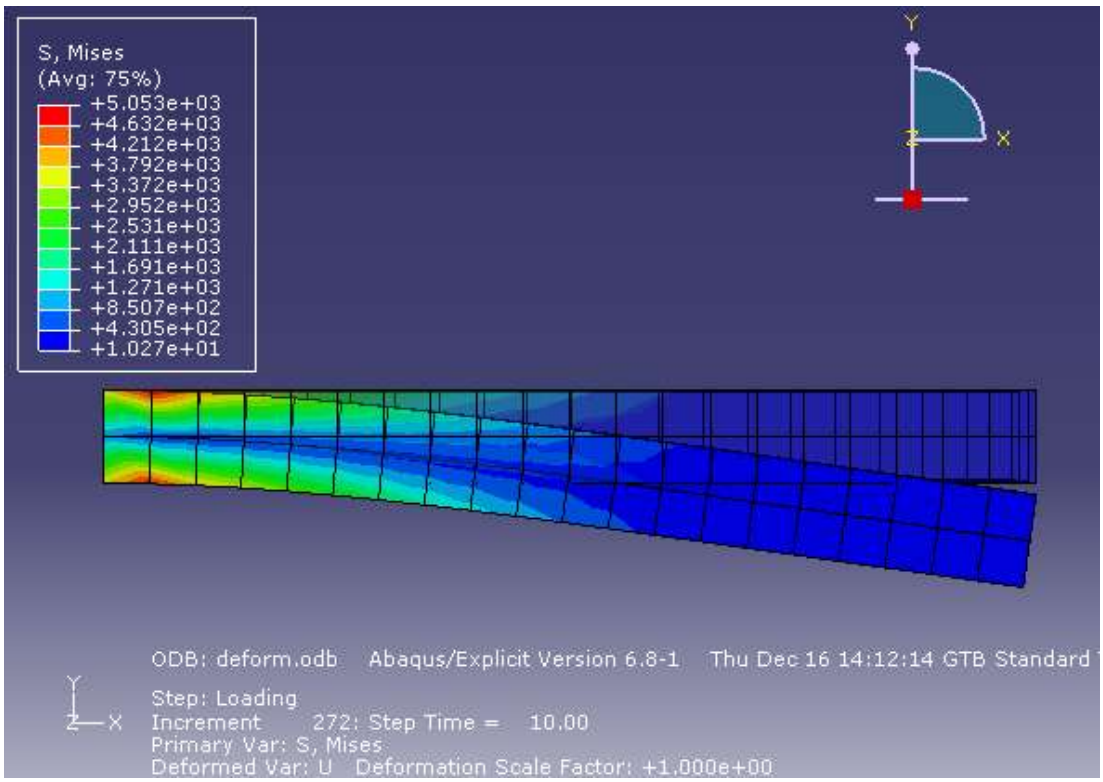

Figure 5.2 : The deformed and undeformed states of the beam model.

The material in the beam model is steel and its elasticity modulus is 209000 GPa. The inverse method program is run with the initial value of 100000 for the elasticity modulus and the direct search routine of Matlab is chosen as the optimization method since there is only one constant to modify. The program tries to make a fit to the fake experimental data generated manually witht the constant 209000 as illustrated in Figure 5.1. In these conditions are inverse FE program, starting from 100000, converged to the value of 208999.76. The quality of the fit with the inversely found constant is given in Figure 5.3.

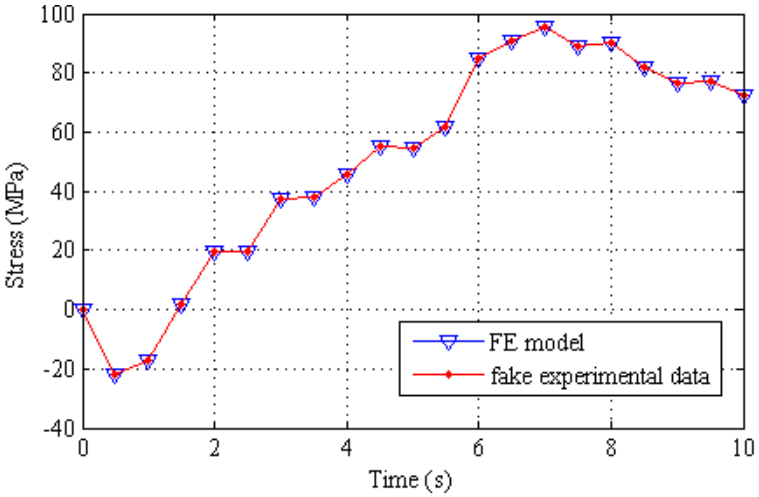

Figure 5.3 : The experimental stress-time data generated manually by the FE tool compared to the stress-time data obtained from the FE model using the inversely determined constant.

The algorithm is also tested for the hyperelasticity case for the Yeoh material model and this time the nonlinear least squares routine of Matlab is used. $C_{10} = 0.000115$, $C_{20} = -0.00007$, and $C_{30} = 0.00115$ are submitted as the initial coefficients of the Yeoh hyperelastic model and the program is run so as to fit the fake experimental data constructed by using the target parameters $C_{10} = 0.0001$, $C_{20} = -0.0001$, and $C_{30} = 0.001$. The ceofficients found as the result of the convergence of the program are $C_{10} = 0.00010426$, $C_{20} = -0.00009456$, and $C_{30} = 0.00092719$. The following figure (Figure 5.4) shows the fit of the inversely found stress curve to the fake experiemental data.

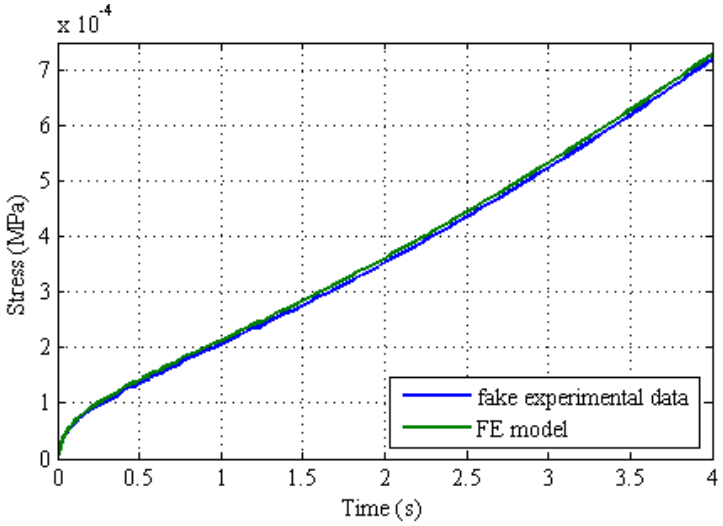

Figure 5.4 : The graph shows the fit of the stress data obtained via inverse FE method to the fake experimental data.

6. RESULTS

The inverse FE jobs are run parallelly on the clusters of the Informatics Institute of ITU. The jobs are submitted to maximum 32 processors. The finite element model codes and the scripts written for the optimization process are given in Appendix A.1 as ready to run on a local machine. The codes given in Appendix A.1 were modified for parallelism.

6.1 AquaFlex Ultrasound Gel Pad

6.1.1 Hyperelastic Model Results

Here in this section, the data obtained from the experiments conducted on the gel pad and the computed parameters of that material both by the inverse FE method and other methods are presented.

For the Aquaflex Ultrasound Gel, the parameters of hyperelasticity are worked out from the static indentation data by four different ways: using Lee & Radok's equation [16], fitting curves to the true stress expressions of Mooney-Rivlin and Yeoh material models and lastly using the inverse finite element method.

Lee and Radok suggested the following equation for the shear modulus:

$$G = 3F / (16\delta\sqrt{R\delta}) \qquad \textbf{(6.1)}$$

Here, G is the shear modulus, δ is the indentation depth and R is the probe radius. Modulus of elasticity, E can also be obtained subsequently, assuming $\upsilon = 0.5$ since the material is assumed to be incompressible via the following relation:

$$G = \frac{E}{2(1+\upsilon)} \qquad \textbf{(6.2)}$$

Using the equations 6.1 and 6.2, Young's modulus values which can be seen in Table 6.1, are obtained from the data of indentations done with three different probes at four different depths.

Table 6.1: Young's (Elastic) modulus of the gel material for various probe radii and displacements.

E (kPa)	Displacement (mm)			
Radius (mm)	2	4	6	8
2	48.4	36.7	45.5	42.1
4	53.9	53.9	61.0	-
6	55.2	57.5	57.2	-

It should be noted that the equation Lee and Radok proposed (Equation 6.1) gives more realistic results in the small deformation cases where $\delta/R << 1$[16]. However, these results also are thought to give an idea about the material's elastic range and assumed to be useful to make an initial approximation of the constants.

Following the elastic approach, the gel data is used in hyperelastic material models. First approach is the Mooney-Rivlin material model of which the strain energy density function is expressed in terms of the first two principal invariants and involves two constants for the incompressible material case (Equation 2.44). The equation is written in terms of true stress as below; how it is transformed is explained in Section 2.3.2.1. The engineering stress (force per unit reference area) is obtained by dividing the true stress by the stretch ratio (Equation 6.4).

$$\sigma = \left(2C_{10} + \frac{2C_{01}}{\Lambda}\right)\left(\Lambda^2 - \frac{1}{\Lambda}\right) \quad \textbf{(6.3)}$$

$$\sigma_{eng} = \left(2C_{10} + \frac{2C_{01}}{\Lambda}\right)\left(\Lambda - \frac{1}{\Lambda^2}\right) \quad \textbf{(6.4)}$$

In this equation, C_{10} and C_{01} are the material coefficients, and I_1 and I_2 are the invariants of the deformation tensor. These coefficients are computed by fitting the static indentation data to the stress expression (Equation 6.3) and the results are given in Table 6.2. One of the fits for which the data was gathered using the 6 mm radius-probe at 6 mm depth is shown in Figure 6.1.

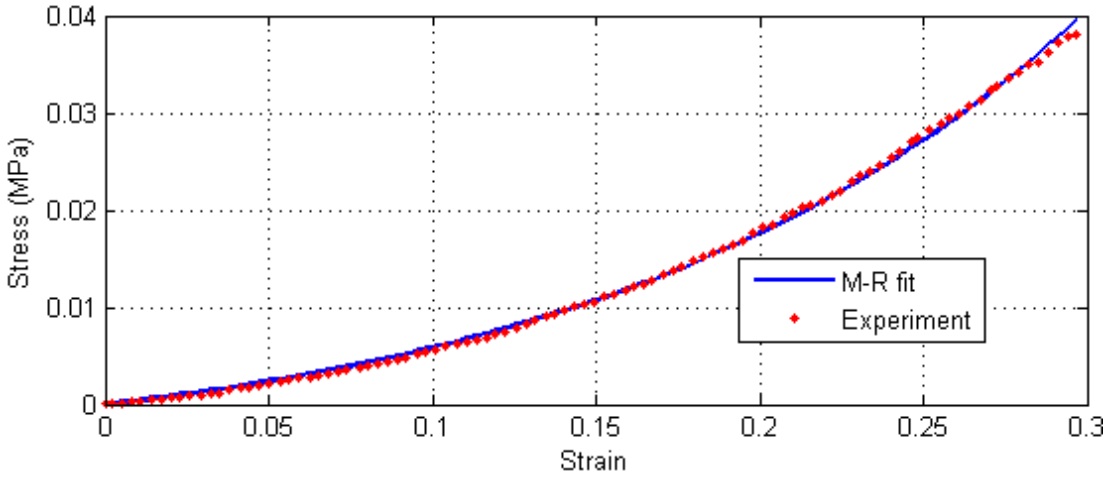

Figure 6.1 : Static indentation test data, conducted by 6 mm radius-probe at 6 mm depth, is fitted to the Mooney-Rivlin material model.

Table 6.2: Coefficients of the strain energy density function for the Mooney-Rivlin material model.

	$R = 2mm$				$R = 4mm$			$R = 6mm$		
	d=2 mm	*d=4 mm*	*d=6 mm*	*d=8 mm*	*d=2 mm*	*d=4 mm*	*d=6 mm*	*d=2 mm*	*d=4 mm*	*d=6 mm*
$C_{01}(MPa)$	-0.3075	-0.1802	-0.0859	-0.0478	-0.0874	-0.0644	-0.0498	-0.0452	-0.0459	-0.0376
$C_{10}(MPa)$	0.2953	0.1667	0.0493	0.0057	0.08	0.0542	0.0354	0.0408	0.0413	0.0324

Mooney-rivlin type strain energy function coefficients are found at both positive and negative values. Negative parameters for this material model are not considered to be physically valid, but there are other studies presenting negative values for the Mooney-Rivlin material model [17]. This may lead to the idea that the strain energy density function is not stable for certain loading conditions since Mooney-Rivlin model best describes rubber-like materials, but here-found negative coefficients fit well to our experimental conditions. However, other hyperelastic material models should be considered. Yeoh material model better reflects the nonlinearity, therefore the curve fitting procedure is also performed for Yeoh material model, using the engineering stress expression (Equation 6.7) which is obtained by dividing the true stress by the stretch ratio (Equation 6.6). Yeoh type strain energy density function is shown in Equation 6.5.

$$W = C_{10}(I_1 - 3) + C_{20}(I_1 - 3)^2 + C_{30}(I_1 - 3)^3 \qquad \textbf{(6.5)}$$

$$\sigma = \left(\Lambda^2 - \frac{1}{\Lambda}\right)\left[2C_{10} + 4C_{20}\left(\Lambda^2 + \frac{2}{\Lambda} - 3\right) + 6C_{30}\left(\Lambda^2 + \frac{2}{\Lambda} - 3\right)^2\right] \quad \textbf{(6.6)}$$

$$\sigma_{eng} = \left(\Lambda - \frac{1}{\Lambda^2}\right)\left[2C_{10} + 4C_{20}\left(\Lambda^2 + \frac{2}{\Lambda} - 3\right) + 6C_{30}\left(\Lambda^2 + \frac{2}{\Lambda} - 3\right)^2\right] \quad \textbf{(6.7)}$$

The results are shown in Table 6.3, Table 6.4, and Table 6.5 for different probe sizes and different depths.

Table 6.3: Coefficients of the strain energy density function of the Yeoh material model, obtained from the test data of 2mm radius probe.

	$R = 2mm$			
	$d = 2mm$	$d = 4mm$	$d = 6mm$	$d = 8mm$
$C_{10}(MPa)$	5.424e-06	1.14e-06	3.66e-10	3.01e-10
$C_{20}(MPa)$	-1.65	-0.4213	-0.2434	-0.1161
$C_{30}(MPa)$	22.48	1.313	0.358	0.08816

Table 6.4: Coefficients of the strain energy density function of the Yeoh material model, obtained from the test data of 4mm radius probe.

	$R = 4mm$		
	$d = 2mm$	$d = 4mm$	$d = 6mm$
$C_{10}(MPa)$	1.201e-04	2.221e-05	1.532e-06
$C_{20}(MPa)$	-0.6852	-0.2149	-0.1089
$C_{30}(MPa)$	10.05	0.7258	0.153

Table 6.5: Coefficients of the strain energy density function of the Yeoh material model, obtained from the test data of 6mm radius probe.

	$R = 6mm$		
	$d = 2mm$	$d = 4mm$	$d = 6mm$
$C_{10}(MPa)$	1.525e-04	4.391e-07	1.288e-05
$C_{20}(MPa)$	-0.3898	-0.1201	-0.05704
$C_{30}(MPa)$	5.725	0.3811	0.07412

The goodness of one of the fits which is the fit to the static indentation data of the test performed by the 6mm radius probe at 6mm depth, is shown in Figure 6.2.

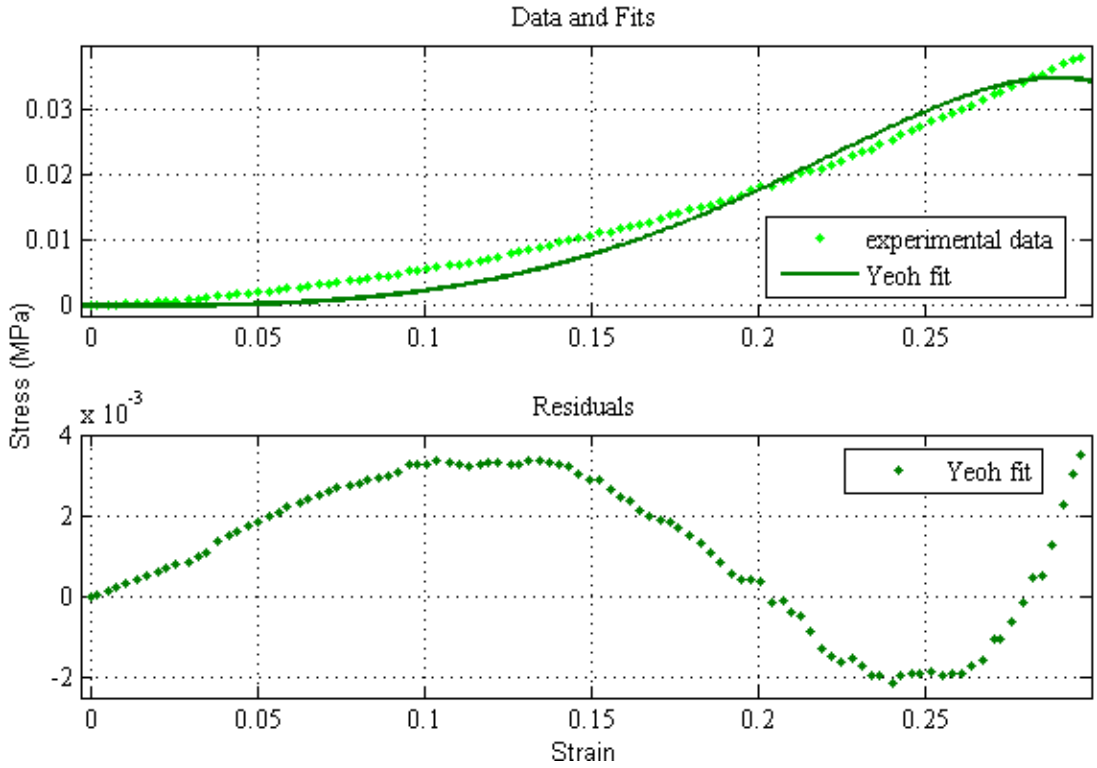

Figure 6.2 : The graph showing the Yeoh material model type curve fitting to the test data of the static indentation with 6mm radius probe at 6mm depth (on the aqua gel), and the residuals of the fit.

6.1.1.1 Inverse FE Method Results

Some constraints are applied for curve fitting; the first coefficient is restricted to be greater than zero, because a negative C_{10} value is not accepted by the finite element tool, causes the *bad material definition* error.

The last method to determine the material results is the inverse algortihm, which is the main subject of this thesis. The results above are aimed to be used in this algorithm in order to set good initial parameters since initial parameters have a key role in convergence of the inverse algorithm. However, this approach didn't work for all cases, so the initial parameters were set regardless of the curve fitting results for some cases.

- Compuatations using the $R = 2mm,\ d = 4mm$ static indentation data:

The resultant coefficients of curve fitting are clearly different from the coefficients found vie the inverse FE method, and the inversey found coefficients also show great differences. This may be caused by some theoretical difference of the finite element tool in defining the material model, which was chosen Yeoh for this case, if the curve fitting results are compared to the inverse method results.

Table 6.6: The coefficients found via inverse FE method, starting with the given initial values, and the coefficients found via curve fitting method.

	C_{10}	C_{20}	C_{30}
Initial coefficients - case 1	0.001	0.001	0.001
Inverse FE results - case 1	0.001376	0.004173	0.002524
Initial coefficients - case 2	0.01	0.01	0.01
Inverse FE results - case 2	0.003554	-0.011223	0.020003
Initial coefficients - case 3	0.000021	0.000199	0.000331
Inverse FE results - case 3	0.001456	0.003688	0.003028
Curve fitting results	1.14e-06	-0.4213	1.313

One more point that should be noted is that the solution is not unique for these kind of fitting problems and in the inverse method it is highly related to the initial values. Though, the following graph shows how well the stres-time curve generated by using the coefficients found via the inverse FE method fits to the curve of the experimental data (Figure 6.3).

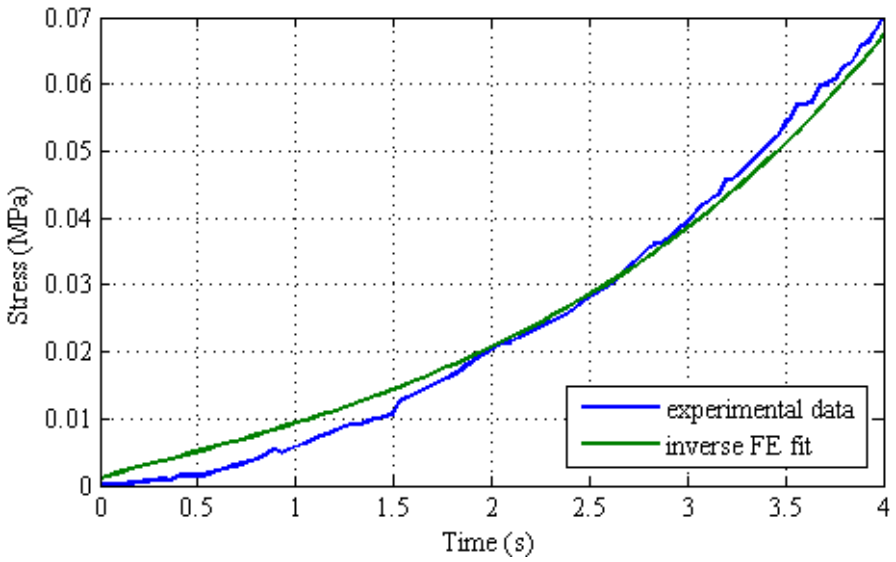

Figure 6.3 : The graph comparing the stress-time curve generated with the inversely found coefficients (case 1) to the real (obtained from experimental data) stress-time curve.

The following graph (Figure 6.4) also illustrates the results for the same conditions, but for case 2, in which the inital values were set different than those of case 1.

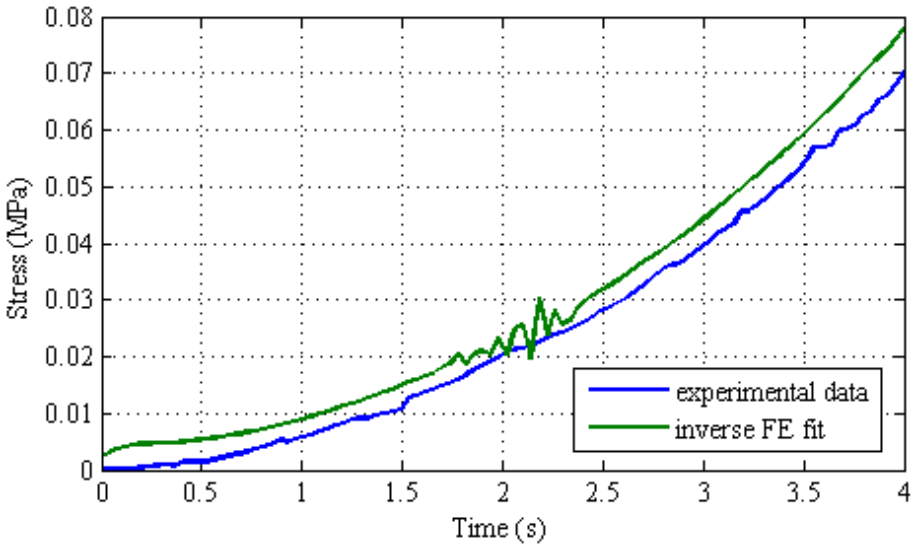

Figure 6.4 : The graph comparing the stress-time curve generated with the inversely found coefficients (case 2) to the real (obtained from experimental data) stress-time curve.

Case 3 also presents different coefficients; the goodness of the fit is shown below in Figure 6.5.

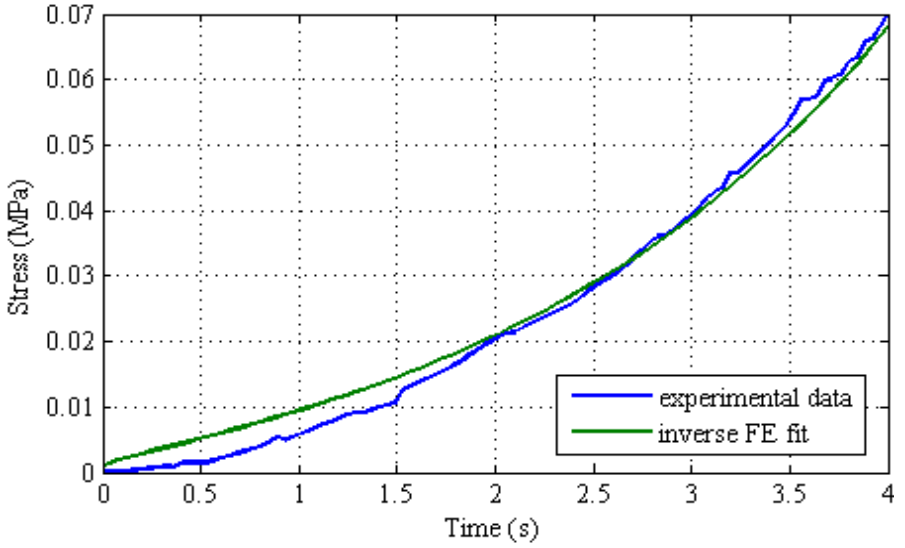

Figure 6.5 : The graph comparing the stress-time curve generated with the inversely found coefficients (case 3) to the real (obtained from experimental data) stress-time curve.

- Compuatations using the $R = 2mm,\ d = 8mm$ static indentation data:

Figure 6.6 is the graph showing the inverse fit that uses the coefficients in Table 6.7 and the experimental data.

Table 6.7: The coefficients found via inverse FE method, starting with the given initial values, and the coefficients found via curve fitting method.

	C_{10}	C_{20}	C_{30}
Initial coefficients	0.01	0.0001	0.0001
Inverse FE results	0.008285	-0.001175	0.000405
Curve fitting results	3.01e-10	-0.1161	0.08816

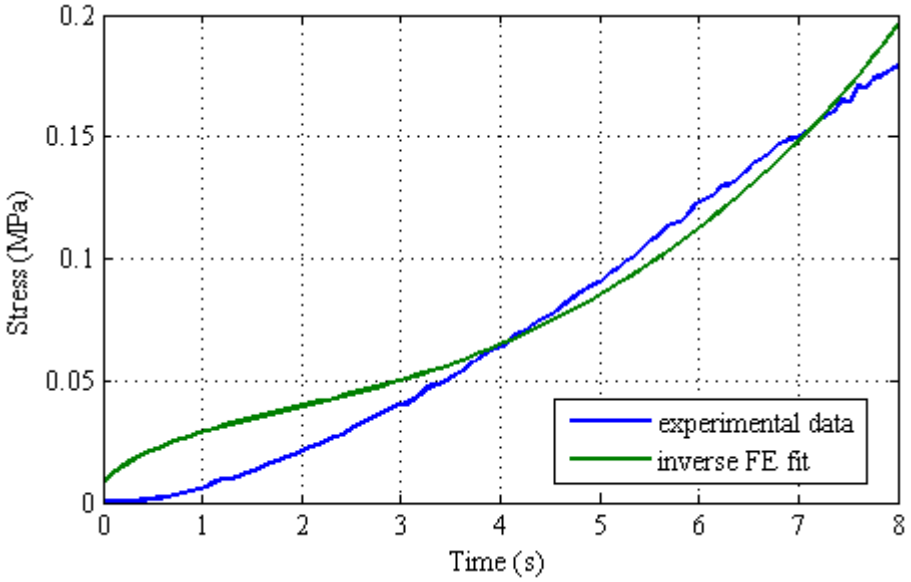

Figure 6.6 : The graph comparing the stress-time curve generated with the inversely found coefficients to the real (obtained from experimental data) stress time curve.

- Compuatations using the $R = 4mm,\ d = 6mm$ static indentation data:

Table 6.8: The coefficients found via inverse FE method, starting with the given initial values, and the coefficients found via curve fitting method.

	C_{10}	C_{20}	C_{30}
Initial coefficients	0.001	0.001	0.001
Inverse FE results	0.001311	0.006561	-0.000795
Curve fitting results	1.532e-06	-0.1089	0.153

Below is the graph showing the inverse fit that uses the coefficients in Table 6.8 and the experimental data (Figure 6.7).

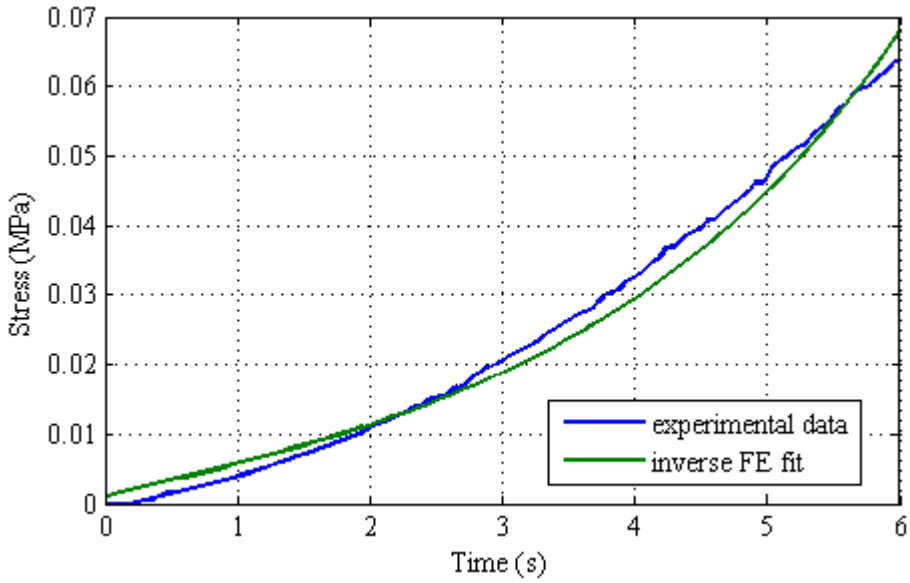

Figure 6.7 : The graph comparing the stress-time curve generated with the inversely found coefficients to the real (obtained from experimental data) stress time curve.

The degree difference in the results which is about $O(10^3)$ is thought to be caused by the unit of density set in the abaqus model. The unit is used as kg/mm^3, however it would be more precise to set it in the unit of $tonne/mm^3$ when the other units are chosen as $N, mm,$ and $MPa.$

6.1.2 Viscoelastic Model Results

The materials are assumed as linearly viscoelastic because the finite element solver can only handle linear viscoelasticity. Linear viscoelasticity is explained in Section 2.3.2 and the model is given in Equation 2.57.

Most commonly used relaxation function that is embedded in the viscoleastic models is Prony series approach; the relaxation fuction expressed as Prony series is given in the following equation:

$$g(t) = E_0(1 - \sum_{i=1}^{n} p_i(1 - e^{-t/\tau_i})) \qquad \textbf{(6.8)}$$

In Equation 6.8, E_0 is the instantaneous modulus of the material, that is the modulus of elasticity, p_i is the i'th Prony constant $(i = 1, 2, ...)$, and τ_i is the i'th Prony retardation time constant $(i = 1, 2, ...)$ [18]. The values for E_0 are taken from the Table 6.1.

Using this approach, relaxation test data is fitted to the Prony series function with $i = 2$ and the above defined parameters are determined.

Table 6.9: Coefficients of the relaxation function for various probe radii and displacements.

	$R = 2mm$ $d = 2mm$	$R = 4mm$ $d = 2mm$	$R = 4mm$ $d = 4mm$
$p_1(MPa)$	0.2023	0.0725	0.115
$p_2(MPa)$	0.2795	0.7325	0.6349
$\tau_1(s)$	13.72	0.5407	1.011
$\tau_2(s)$	302.2	168.6	149.4

Below is the graph showing the goodness of fit for two cases; the Prony series is expanded with 2 set of unknowns for the first, and expanded with 3 set of unknowns for the second case. Here, these unknowns are the coefficients that are aimed to be determined.

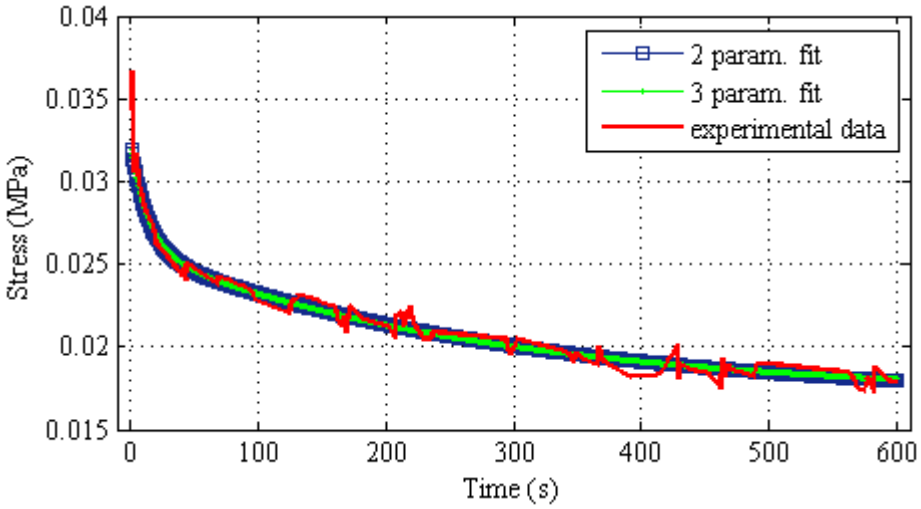

Figure 6.8 : Nonlinear curve fitting with the 2 and 3-parameter Proney series model, fitted to the relaxation test data; probe radius is 2mm, indentation depth is 2mm and the hold time is 600 s.

6.2 Bovine Liver

6.2.1 The Effect of Storing The Liver in Serum Liquid

The results of the experiments are illustrated in the third chapter; however the effect of storage conditions of the liver is not given yet. The static indentation and ramp-hold test results given in the previous chapter belong to the liver which had been kept in a serum liquid right after it was removed from the animal until it was subjected to material testing. We also have test data of a liver which hadn't been kept in the fluid before testing. The following figures show the difference in the data caused by the storage conditions.

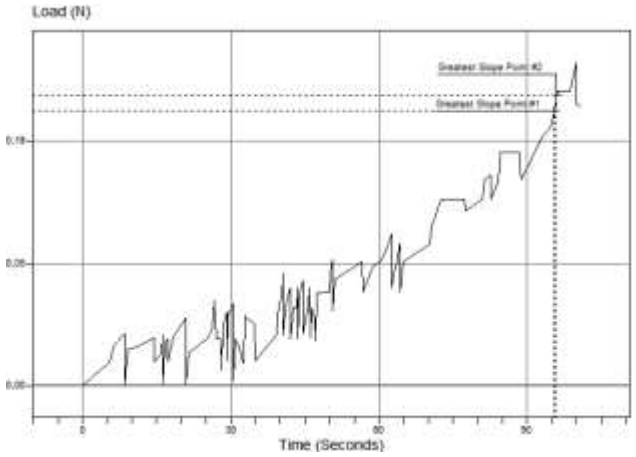

(a)

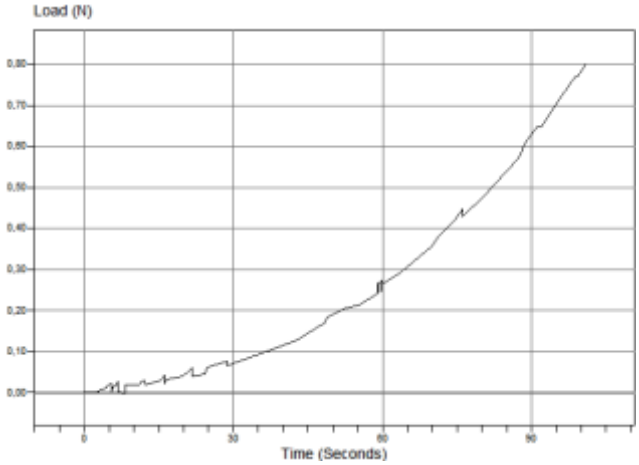

(b)

Figure 6.9 : The static indentation data of the tests conducted by the probe of 4mm radius to the depth of 10mm, on the liver stored (a) not within serum, and (b) within serum.

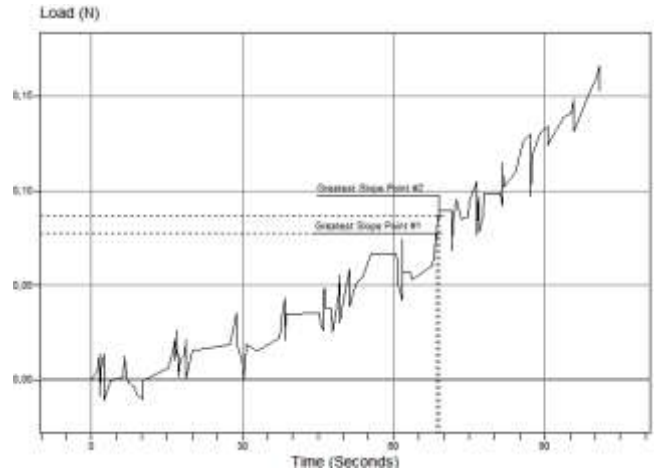

(a)

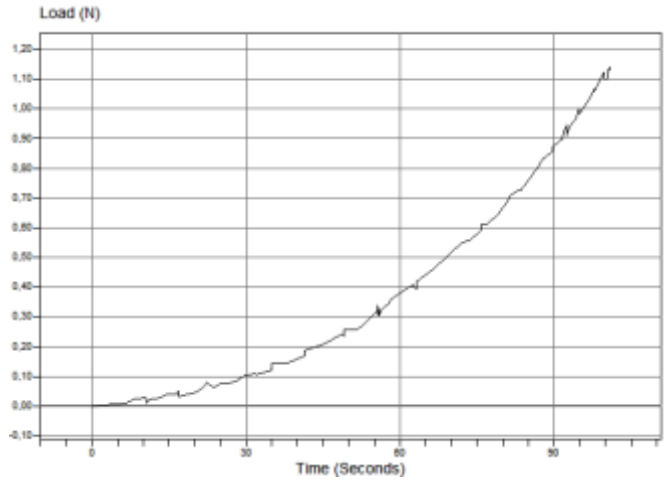

(b)

Figure 6.10 : The static indentation data of the tests conducted by the probe of 6mm radius to the depth of 10mm, on the liver stored (a) not within serum, and (b) within serum.

At both group of tests, that is, at the tests with the probe of 4mm radius or 6mm radius, the curves demonstrate that there is a difference in the force response between the liver stored in the serum liquid and the one not stored in it; the force response of the liver stored in the liquid is clearly greater. However, the fact that each distinct liver taken out from a different animal may feature difference in structure and in mechanical properties should be in mind, even if they are from the same species.

6.2.2 Hyperelastic Model Results

The method that had been proposed by Lee and Radok [16] is used again with the static indentation data gathered from the liver material tests. Equation 6.1 and Equation 6.2 are used; the results are presented in Table 6.10.

Table 6.10: Young's (Elastic) modulus of the bovine liver for various probe radii and displacements.

E (kPa)	Displacement (mm)			
Radius (mm)	4	6	8	10
2	5.809	5.014	5.551	5.227
4	4.768	4.259	4.121	5.097
6	3.930	5.783	5.690	5.726

The data shown in Table 6.10, when compared to the data in Table 6.1, briefly demonstrates that the elastic response of bovine liver and the ultrasound aquaflex gel do not look alike since the estimated elastic moduli are not in a similar range.

The static indentation data obtained from tests on liver are again used in stress expression of the Yeoh type hyperelastic material model (Equation 6.7) as it is done for the ultrasound aqua gel material. The stretch ratios are calculated using the liver thickness data which had been measured and recorded at each indentation, since the dimensions of liver were not constant at each point differently from the gel.

The following tables (Table 6.11, Table 6.12, and Table 6.13) shows the coefficients found by the curve fitting method using the stress expression in Equation 6.7:

The graphs in Fgure 6.11 shows the goodness of the fit for one test case.

Table 6.11: Coefficients of the strain energy density function of the Yeoh material model, obtained from the test data of 2mm radius probe.

	$R = 2mm$			
	$d = 4mm$	$d = 6mm$	$d = 8mm$	$d = 10mm$
$C_{10}(MPa)$	2.225e-14	2.22e-14	3.945e-06	1.782e-06
$C_{20}(MPa)$	-5.534	-2.865	-2.203	-0.5836
$C_{30}(MPa)$	442.2	72.59	31.31	2.573

Table 6.12: Coefficients of the strain energy density function of the Yeoh material model, obtained from the test data of 4mm radius probe.

	$R = 4mm$			
	$d = 4mm$	$d = 6mm$	$d = 8mm$	$d = 10mm$
$C_{10}(MPa)$	2.22e-14	4.01e-05	4.436e-07	7.923e-07
$C_{20}(MPa)$	1.86	-0.8747	-0.4574	-0.3588
$C_{30}(MPa)$	137.1	23.3	5.531	2.528

Table 6.13: Coefficients of the strain energy density function of the Yeoh material model, obtained from the test data of 6mm radius probe.

	$R = 6mm$			
	$d = 4mm$	$d = 6mm$	$d = 8mm$	$d = 10mm$
$C_{10}(MPa)$	0.0001376	1.636e-05	1.33e-05	1.256e-06
$C_{20}(MPa)$	-1.017	-0.591	-0.3906	-0.2949
$C_{30}(MPa)$	70.57	15.94	5.4	2.309

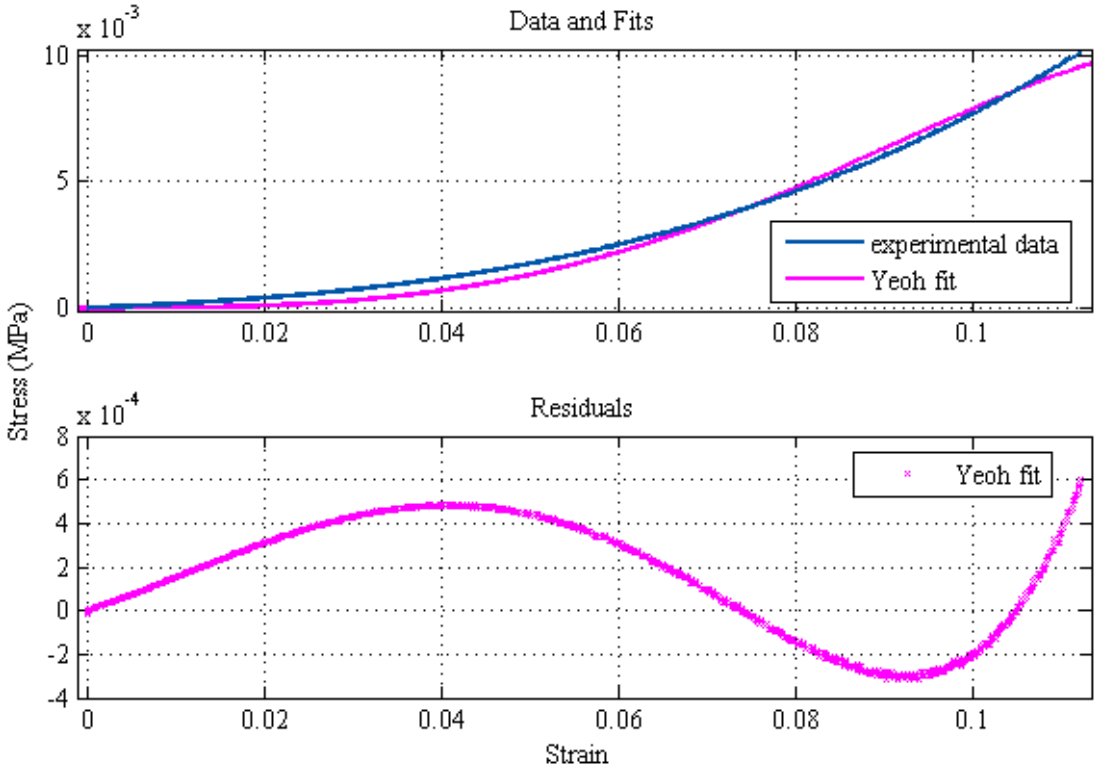

Figure 6.11 : The graph showing the Yeoh material model type curve fitting to the test data of the static indentation with 6mm radius probe at 10mm depth (on liver), and the residuals of the fit.

6.2.2.1 Inverse FE Method Results

For the inverse finite element method jobs the constraint that keeps the first coefficient of the Yeoh material model is again used, because a negative C_{10} value causes the *bad material definition* error by the finite element tool.

The FE model is reconstructed, because the thickness of the bovine liver changed at each case. The FE model is altered according to thickness, which is directly invlolved in strain definiton.

Below is the result of the inverse FEM; the coefficients computed via inverse FEM are shown in the table and the fit is graphed.

- Compuatations using the $R = 4mm,\ d = 4mm$ static indentation data:

Table 6.14: The coefficients found via inverse FE method, starting with the given initial values, and the coefficients found via curve fitting method.

	C_{10}	C_{20}	C_{30}
Initial coefficients	0.001	0.001	0.001
Inverse FE results	0.000149	-0.000160	0.013708
Curve fitting results	2.22e-14	1.86	137.1

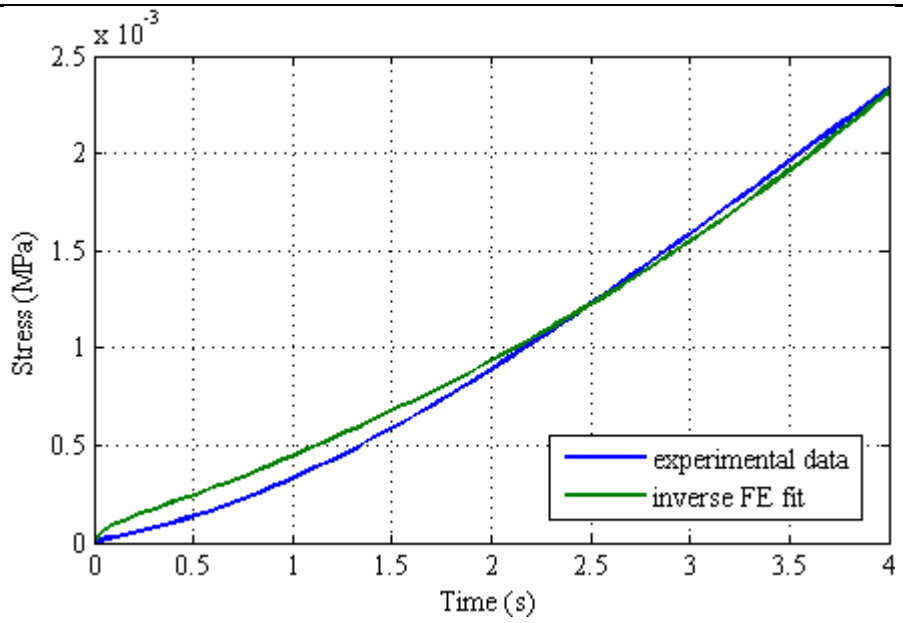

Figure 6.12 : The graph comparing the stress-time curve generated with the inversely found coefficients to the experimental stress-time curve of the bovine liver, for the case of $R = 4mm,\ d = 4mm.$

Figure 6.12 is the graph showing the inverse fit that uses the coefficients in Table 6.14 and the experimental data.

- Compuatations using the $R = 4mm,\ d = 6mm$ static indentation data:

Table 6.15: The coefficients found via inverse FE method, starting with the given initial values, and the coefficients found via curve fitting method.

	C_{10}	C_{20}	C_{30}
Initial coefficients	0.00001	0.00008	0.00233
Inverse FE results	0.000119	-0.0000003	0.002396
Curve fitting results	4.01e-05	-0.8747	23.3

Below is the graph showing the inverse fit that uses the coefficients in Table 6.15 and the experimental data (Figure 6.13).

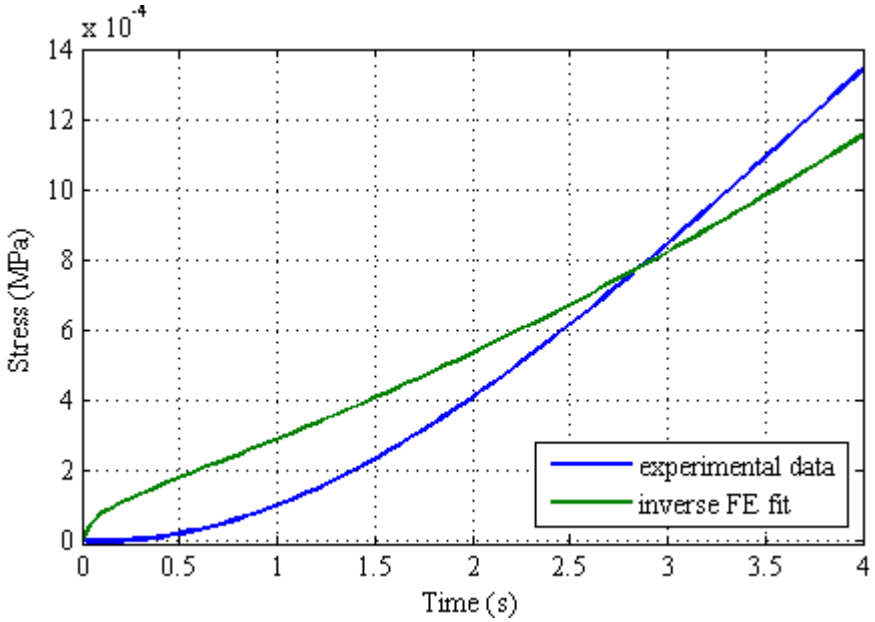

Figure 6.13 : The graph comparing the stress-time curve generated with the inversely found coefficients to the experimental stress-time curve of the bovine liver, for the case of $R = 4mm,\ d = 6mm.$

6.2.3 Viscoelastic Model Results

The Prony series relaxation function approach for the viscoelastic model is also used with the liver test data. Curve fitting is done using the Prony series expansion with 3 parameter sets (Equation 6.8).

The calculated parameters are given in tables below. The following table gives the parameters for the test case performed by the 2mm-radius probe. The indentation depths for that case are 4mm, 6mm, and 8mm.

Table 6.16: Coefficients of the relaxation function for various probe radii and displacements for the case of $R = 2$ of bovine liver tests.

	$d = 4mm$	$d = 6mm$	$d = 8mm$
$p_1(MPa)$	0.613	-3.069	-6.263
$p_2(MPa)$	1.579	3.286	6.38
$p_3(MPa)$	-1.411	-3.867	-7.061
$\tau_1(s)$	0.1245	0.1245	0.1245
$\tau_2(s)$	76.28	79.57	80.05
$\tau_3(s)$	0.067	0.067	0.067

Table 6.17 presents the parameters for the 4mm-radius case at which the tests are conducted to the 4mm, 6mm, and 8mm depths on the bovine liver.

Table 6.17: Coefficients of the relaxation function for various probe radii and displacements for the case of $R = 4$ of bovine liver tests.

	$d = 4mm$	$d = 6mm$	$d = 8mm$
$p_1(MPa)$	0.09031	-0.6603	-1.696
$p_2(MPa)$	0.9256	1.526	2.387
$p_3(MPa)$	-0.7076	-1.458	-2.493
$\tau_1(s)$	0.1245	0.1245	0.1245
$\tau_2(s)$	21.38	45.06	79.93
$\tau_3(s)$	0.067	0.067	0.067

Table 6.18 gives the parameters for the 6mm-radius case at which the tests are conducted to the 4mm, 6mm, and 8mm depths on the bovine liver.

Table 6.18: Coefficients of the relaxation function for various probe radii and displacements for the case of $R = 6$ of bovine liver tests.

	$d = 4mm$	$d = 6mm$	$d = 8mm$
$p_1(MPa)$	0.4253	0.3522	-0.05648
$p_2(MPa)$	0.6685	0.6581	0.8614
$p_3(MPa)$	-0.3726	-0.4457	-0.8543
$\tau_1(s)$	0.1245	0.1245	0.1245
$\tau_2(s)$	10.58	14.49	44.71
$\tau_3(s)$	0.067	0.067	0.067

The goodness of the fits are illustrated in the graphs below.

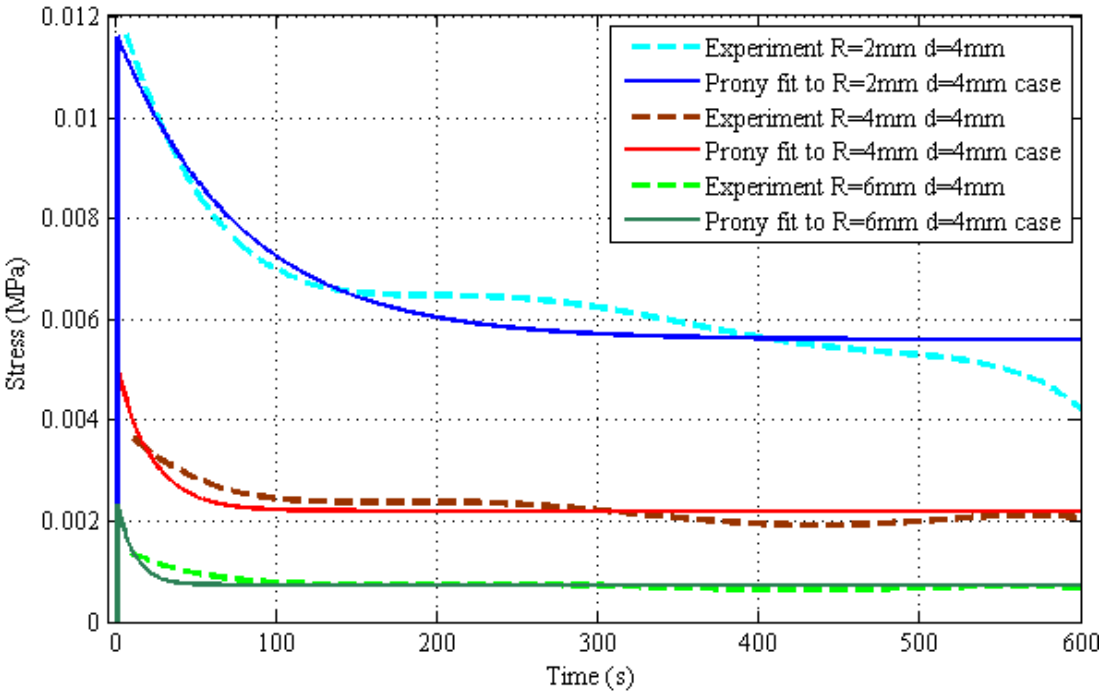

Figure 6.14 : Prony series approach for the relaxation function is fitted to the ramp hold data of the bovine liver for the case of $d = 4mm$.

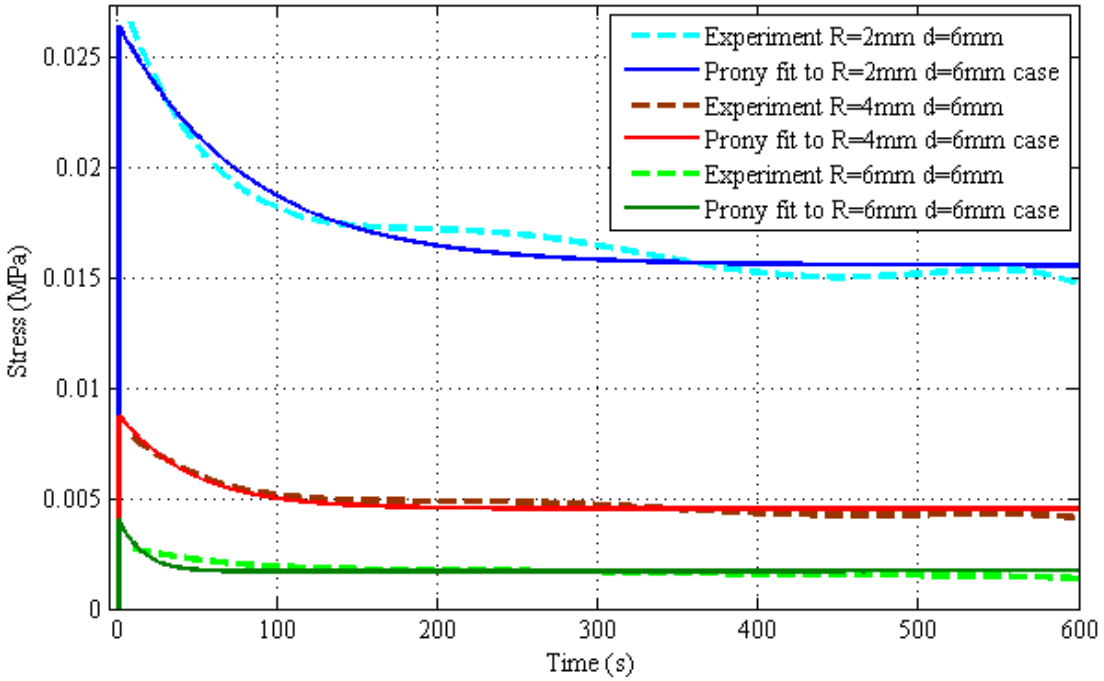

Figure 6.15 : Prony series approach for the relaxation function is fitted to the ramp hold data of the bovine liver for the case of $d = 6mm$.

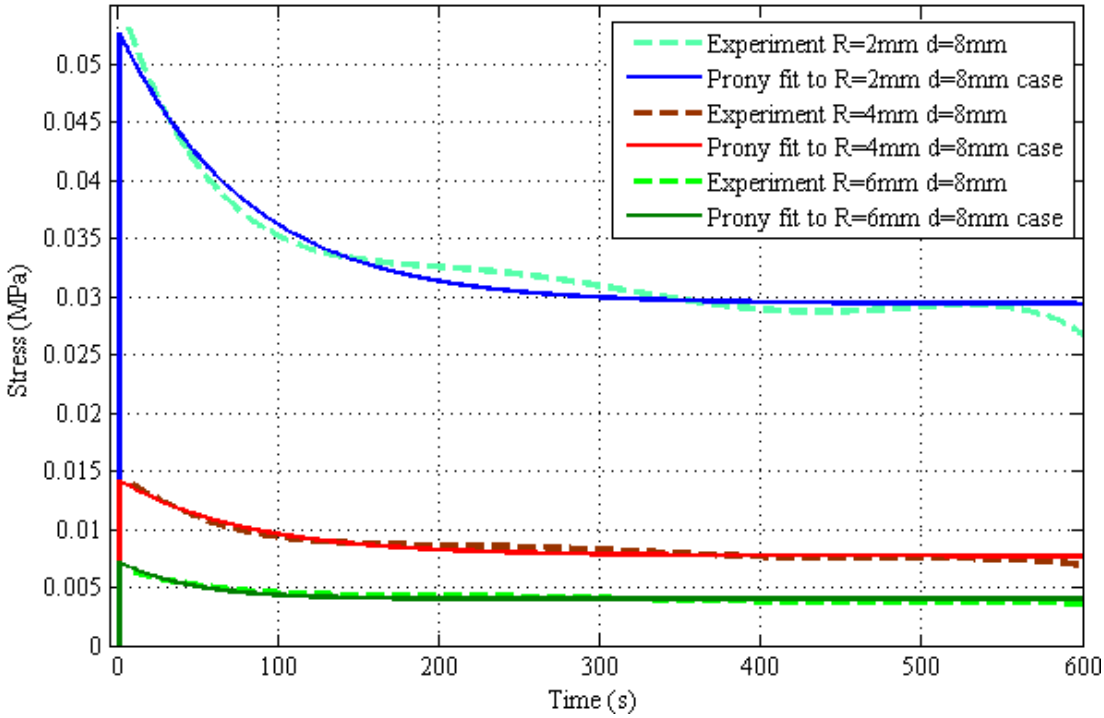

Figure 6.16 : Prony series approach for the relaxation function is fitted to the ramp hold data of the bovine liver for the case of $d = 8mm$.

6.3 Comparing the Mechanical Properties of Aquaflex Ultrasound Gel and Bovine Liver

Even though, the method that Lee and Radok had proposed had been constructed for small deformation cases [16], the obvious difference between the data given in Table 6.1 and Table 6.10 can inform us that the synthetic material that was subjected to material testing in this study, do not resemble mechanically to the bovine liver. The effective elastic modulus of the bovine liver seems averagely one order of magnitude smaller than that of the synthetic material.

7. CONCLUSION

The method of estimating the material coefficients of soft biological tissues by inverse finite element method is dealed in this study and the resources of the inverse finite element method is provided with an experimental work. The experiments are designed as static indentation tests and ramp-hold tests. Tests are performed on two materials; one is a synthetic material, Aquaflex Ultrasound Gel Pad, the second one is the bovine liver. The data obtained from the material tests are used in the computations of the material coefficients that take place in the equations of the material models, which are chosen as Yeoh type hyperelastic and linear viscoelastic.

The tests on the synthetic material demonstrated the mechanical properties of the material; it is seen to have a nonlinear stress-strain relation. The ramp-gold tests showed the relaxation characteristic of the material and this property lead us to model it as viscoelastic. The bovine liver is already known for its nonlinear viscoelastic behaviour as it is a soft biological tissue.

Another set of material tests are performed in order to examine the axial differentiation in the mechanical behaviour of the bovine liver. The static indentation tests conducted on the orthogonal faces of a cubic bovine liver part showed the anisotropy of the tissue by exhibiting different force responses for the same test cases. However, the heterogenity of the tissue is also seen as an important parameter to consider since the replicated tests on the same face but on different points could produced different data.

Other than the material test data of the bovine liver that is used in this study for coefficient estimation, a previous data set that had been obtained from another bovine liver which had not been kept in serum fluid, is used for the comparison of these two groups of data, resulting that the storing condition made sense.

The coefficients are calculated via both curve fitting and inverse FE method. It has been concluded that the results obtained from the inverse FE method is strictly depend on the initial parameters given to the algorithm. Curve fitting results helped

to decide the initial parameters for some cases but not for all. There have been an obvious degree difference between the results of the curve fitting method and inverse FEM which is later understood to have been caused by the inconsistent unit usage for the density.

Some parts of the work done during this thesis, the experimental work and the curve fitting results, are published in some conferences both national and international. These proceedings are referenced in [19], [20], and [21].

In this study, the overall structure of the inverse FE method is constructed; finite element models are created, the algorithm is coded, the program converged and computed the coefficients. It can be seen that the the results of the curve fitting method differ from the results of the inverse FEM. This suggests that the parameter estimation by both methods needs further improvement in terms of finite element modeling and in terms of material description. The overall model can be improved for the case of nonlinear viscoelastic materials. The results already show that not every hyperlastic material model fit to the soft tissue materials; it is seen in this study that Yeoh model is more suitable than Mooney-Rivlin model however Yeoh also fails to give a good fit in case of large deformations. Therefore, choosing a more suitable hyperleastic material model or defining a new material model can be performed as a future improvement.

REFERENCES

[1] **Carter, F. J., Frank, T. G., Davies, P. J., McLean, D. and Cuschieri, A.,** 2001: Measurements and modelling of the compliance of human and porcine organs. *Medical Image Analysis*, Vol. **5**, no. 4, pp. 231-236.

[2] **Kim, J. and Srinivasan, M. A.**, 2005: Characterization of Viscoelastic Soft Tissue Properties from In Vivo Animal Experiments and Inverse FE Paramter Estimation. Medical Image Computing and Computer-Assisted Intervention – MICCAI 2005, 8th International Conference, Part II, October 26-29, 2005, Palm Springs, CA, USA.

[3] **Kerdok, A. E., Ottensmeyer, M. P. and Howe, R. D.,** 2006: Effects of perfusion on the viscoelastic characteristics of liver. *Journal of Biomechanics*, Vol. **39**, pp. 2221-2231.

[4] **Ottensmeyer, M. P., Kerdok, A. E., Howe, R. D. and Dawson, S. L**., 2004: Proceedings of Medical Simulation: International Symposium – ISMS 2004, June 17-18, 2004, Cambridge, MA, USA.

[5] **Kerdok**, **A. E., Cotin, S. M., Ottensmeyer, M. P., Galea, A. M., Howe, R. D. and Dawson, S. L.,** 2003: Truth cube: Establishing physical standards for soft tissue simulation. *Medical Image Analysis*, Vol. **7**, pp. 283-291.

[6] **Dogan, F. and Celebi, M. S.,** 2010: Real-time deformation simulation of non-linear viscoelastic soft tissues. *Simulation*, doi:10.1177/0037549710364532.

[7] **Holzapfel, G. A.,** Nonlinear Solid Mechanics: A Continuum Approach for Engineering, John Wiley & Sons Ltd., England.

[8] **Shabana, A. A.,** Computational Continuum Mechanics, Cambridge University Press, USA.

[9] **Fung, Y. C.,** Biomechanics: Mechanical Properties of Living Tissues, 2nd Edition, Springer-Verlag, New York, USA.

[10] **Humphrey, J. D.,** Cardiovascular Solid Mechanics, Cells, Tissues and Organs, Springer-Verlag, New York, USA.

[11] **Provenzano, P., Lakes, R., Keenan, T. and Vanderby, R, Jr.,** 2001: Nonlinear ligament viscoelasticity. *Annals of Biomedical Engineering*, Vol. 29, pp. 908-914.

[12] **Dessault Systèmes,** 2010: Abaqus Documentation Collection

[13] **Kauer, M.,** 2001: Inverse finite element characterization of soft tissues with aspiration experiments. Diss. ETH No. 14233, Swiss Federal Institute of Technology.

[14] **Aster, R. C., Borchers, B. and Thurber, C. H.,** Parameter Estimation and Inverse Problems, Boston: Elsevier Academic Press, USA.

[15] **Url-1** < *http://www.applied-mathematics.net/LMvsTR/LMvsTR.html* >, accessed at 20.12.2010.

[16] **Lee, E. H. and Radok, J. R. M.,** 1960: The contact problem for viscoelastic bodies. *Journal of Applied Mechanics*, Vol. 27, pp. 438-444.

[17] **Hu, T. and Desai, J. P.,** 2004: Characterization of Soft-Tissue Material Properties: Large Deformation Analysis. Medical Simulation International Symposium, ISMS 2004, June 17-18, 2004 Cambridge, MA, USA.

[18] **Chen, T.,** 2000: Determining a Prony Series for a Viscoelastic Material From Time Varying Strain Data. NASA Technical Report, TM-2000-210123 ARL-TR-2206.

[19] **Dogan, F., Demir, G., Celebi, M. S.,** 2010: Indentation Experiments on Viscoelastic Gel Material for Validating Medical Simulations. *The 15th National Biomedical Engineering Meeting*, April 21-24, 2010 Antalya, Turkey.

[20] **Demir, G., Dogan, F., Celebi, M. S.**, 2010: Calculation of Material Coefficients of a Viscoelastic Gel for Validationg Soft Tissue Deformations. *The V. National Biomechanics Congress,* September 23-25, 2010 Izmir, Turkey.

[21] **Demir, G., Dogan, F., Celebi, M. S**., 2010: Determination of Material Constants of Viscoelastic Gel for Validating Soft Tissue Simulations. *The 2010 International Congress on Computer Applications and Computer Science*, December 04-06, 2010 Singapore.

[22] **Mecitoglu, Z.**, 2008: Finite element analysis in structures: course notes, Istanbul Technical University, Turkey, < *http://web.itu.edu.tr/~mecit/*> accessed at 15.01.2010.

[23] **Url-2** <*http://en.wikiversity.org/wiki/File:Motion.png*>, accessed at 10.12.2010.

[24] **Url-3** <*http://library.kiwix.org:4201/A/Stress_physics_.html*>, accessed at 10.12.2010.

[25] **Gere, J. M., Goodno, B. J.,** Mechanics of Materials, Seventh Edition, Cengage Learning, USA.

[26] **Url-4** <*http://www.scielo.cl/scielo.php?pid=S0718-221X2009000100002&script=sci_arttext*>, accessed at 10.12.2010.

[27] **Url-5** <*http://geuz.org/gmsh* >, accessed at 10.12.2010.

APPENDICES

APPENDIX A.1 : The inverse finite element method codes:

submit_matlab.m: The Matlab script that starts the algorithm and runs the optimization routine.

myresiduals.m: The Matlab function that runs the finite element model job and computes the residuals between the experimental data and model data.

litcount.m: The Matlab function that embeds the new parameters into the Abaqus input file.

openodb.py: The python script that selects the required data from the finite element model database file.

APPENDIX A.1

myresiduals.m :

```
function err = myresiduals_p(params)

format long
fid = fopen('params.txt','a');
measfile = ('liver_r6d4.dat');
h_meas = load(measfile);
h_abaqus = load('s22_abaqus.dat');
err = h_meas-h_abaqus

fprintf(fid, '%.15f %.15f %.15f %.15f %.15f %.15f\n', params(1),
params(2), params(3), 0, 0, 0);

fclose(fid);
end
```

submit_matlab.m :

```
clear; clc;

params = [0.001, 0.001, 0.001];
options = optimset('TolX', 1e-8, 'TolFun', 1e-8, 'MaxIter',
1000);

[res_params,fval,exitflag,output] = lsqnonlin(@myresiduals,
params, [0, -Inf, 0], [], options);
res_params
fval
exitflag
output
```

litcount.m :

```
function litcount(filename, literal, params)

% Search for a string
format long;
fid = fopen(filename);
[newF,message]=fopen('test_tmp.inp','w');
tline = fgetl(fid);

while ischar(tline)
   matches = strfind(tline, literal);
   num = length(matches);

    if num > 0
        fprintf(newF, '*Hyperelastic, yeoh\n');
        fprintf(newF, '%.33f, %.33f, %.33f, %f, %f, %f\n',
params(1), params(2), params(3), 0, 0, 0);
        fgetl(fid);
    else
        fprintf(newF,tline);
        fprintf(newF,'\n');
```

```
    end
    tline = fgetl(fid);
end
fclose(newF);
copyfile('test_tmp.inp', filename);
fclose(fid);
end
```

openodb.py :

```
from odbAccess import *

odb = openOdb(path='job1.odb')
file = open('s22_abaqus.dat','w')

myframes=odb.steps['Step-1'].frames

# values[99] is the 100st element in the model
# data[1] gives the 2nd stress component(S22) in the y-direction
for i in myframes:
    s22data = (-1)*(i.fieldOutputs['S'].values[99].data[1])
    file.write(str(s22data) + '\n')

file.close()
odb.close()
```

CURRICULUM VITAE

Candidate's full name: **Gülnur Demir**

Place and date of birth: **Mainz/B.Almanya 24.01.1984**

Permanent Address: **Esenevler m. Yunus Emre c. Mücahit s. No:5/4 Ümraniye İstanbul TURKEY**

Universities and Colleges attended: **Istanbul Technical University, Mathematical Engineering (2002-2006)**

Publications:

- **Demir, G.,** Dogan, F., Celebi, M. S., 2010: Determination of Material Constants of Viscoelastic Gel for Validating Soft Tissue Simulations. *The 2010 International Congress on Computer Applications and Computer Science*, December 04-06, 2010 Singapore.

- **Demir, G.,** Dogan, F., Celebi, M. S., 2010: Calculation of Material Coefficients of a Viscoelastic Gel for Validationg Soft Tissue Deformations. *The 5th National Biomechanics Congress*, September 23-25, 2010 Izmir, Turkey.

- Dogan, F., **Demir, G.,** Celebi, M. S., 2010: Indentation Experiments on Viscoelastic Gel Material for Validating Medical Simulations. *The 15th National Biomedical Engineering Meeting*, April 21-24, 2010 Antalya, Turkey.